



Biogeosciences

Date: June 24, 2016

Subject: Submission of revised manuscript bg-2016-64

Dear Tina,

Hereby we submit the revised manuscript bg-2016-64 “**Anaerobic oxidation of methane alters sediment records of sulfur, iron and phosphorus in the Black Sea**” by Matthias Egger, Peter Kraal, Tom Jilbert, Fatimah Sulu-Gambari, Célia J. Sapart, Thomas Röckmann and Caroline P. Slomp.

We would like to thank the three reviewers for their encouraging and critical remarks that helped to improve our manuscript. With this letter, we have also added a detailed reply to the reviewer’s comments including an explanation of how and where each point raised by the reviewers was incorporated in the manuscript, a list of all relevant changes made in the manuscript, as well as a marked-up manuscript version. We followed the reviewer’s recommendations in most cases.

Please note that all line numbers in our replies refer to the revised text, unless stated otherwise.

Sincerely, on behalf of all authors,

Matthias Egger

Response to reviewers for manuscript bg-2016-64

Referee # 1 (Orit Sivan)

Referee's comment: This paper deals with diagenetic processes in the sediments of the Black Sea which changed from a lacustrine environment to a marine system. The work focuses on AOM and its effect on the linked species and processes under these changes. This was done by producing solid phase and porewater profiles, and by diagenetic modeling. The work is well written and easy to read, and I found it complete, serious and convincing. The authors measured, calculated and thought on almost all the possible aspects that could affect this system during these changes. This careful work enhances our understanding on AOM by iron and sulfate in marine setting in general and specifically in a complex setting. It also provides us with new knowledge on the Black Sea's limnological history. I thus suggest accepting this work pending minor comments.

Author's reply: We thank the referee for the compliment. We reply to the comments below and have now revised the manuscript accordingly.

Referee's comment: The model is not detailed and explained enough. You should cite less Rooze et al 2016 and provide more details here. Also, you should perform sensitivity tests for the various uncertainties. I did not have access to Rooze et al paper, but from its title I am assuming it is not on the same system so there is no overlapping. You should however upload this paper.

Author's reply: We have expanded the model description in the revised version of the manuscript (**lines 247-257**). In addition, we have performed appropriate sensitivity tests and show the uncertainties associated with key processes in the Supplementary Information (see also reply to referees #2 and #3) (**lines 241-243 and Supplementary Figs. S2 and S3**). Note that we changed the model grid from constant to exponentially decreasing (**lines 280-282**). This change had no effect on the results, but helped to speed up the sensitivity analyses. The study by Rooze et al. can be found at <http://onlinelibrary.wiley.com/doi/10.1002/lno.10275/abstract>

Referee's comment: The Fe²⁺ increase in the deep sediments could be from deep Fe-AOM as we see in lakes and coastal sediments (Sivan et al., 2011; Egger et al., 2015), however it can also be organoclastic. There may be reactivation of less soluble Fe(III) minerals in this system by other means other than methane oxidation (e.g as described by Sivan et al., 2016). You indeed mention it, however, you should refer to it as a possible option.

Author's reply: We have clarified that the reactivation of more crystalline Fe oxides by methanogens as described by Sivan et al. (2016) represents a possible mechanism for the Fe reduction at depth in the sediment (**lines 32; 95-96; 606-607 and 1022-1023**).

Referee's comment: The assumption that the total dissolved Fe and Mn (as measured by AE-ICP) are Fe(II) and Mn(II) is probably fine, however you should test it and show it in at least in one of the profiles in the Black sea sediments (or cite other works that did it there). You should compare

the Fe(II) to Fe(total) by another method (as the Ferrozine), or compare your assumed Fe(II) to Fe(II) from the Ferrozine or another method.

Author's reply: Unfortunately, we cannot test this as we acidified our pore water samples prior to analysis for Fe and Mn with ICP-OES. Although the solubility of Fe(OH)₃ is very low at natural pH and the occurrence of dissolved Fe³⁺ is highly unlikely in reducing sediments, Fe(OH)₃ or Fe(OH)²⁺ complexes could pass through the 0.45 μm filters used in this study (Raiswell and Canfield, 2012; *Geochem. Perspect.*). In addition, a small fraction of the dissolved Mn could indeed be present as Mn³⁺, as shown for suboxic surface sediments (Madison et al., 2013; *Science*). We have now included that the dissolved Fe and Mn in our study refers to Fe and Mn passing through a 0.45 μm filter and thus likely consists of a mixture of truly dissolved (aqueous), as well as organically complexed, colloidal and nanoparticulate Fe and Mn species in the method section of the revised manuscript **(lines 146-148)**.

Referee's comment: You should discuss in more detail the sulfate profile and – its apparent “diffusion” profile (linear curve) with organoclastic sulfate reduction, and the cryptic S cycle in the upper part of this profile. You should also compare the downward flux of sulfate to the SMTZ and the upward flux that you calculated for methane and discuss it.

Author's reply: As suggested by the referee, we now discuss the sulfate profile in more detail **(lines 397-404)** and also elaborate on the relative fluxes of sulfate and methane to the SMTZ **(lines 414-418)**.

Referee's comment: The δ¹³C of methane similarity to Yoshinaga's data is convincing and satisfactory. Interpretation/speculations regarding the profile of δD of methane should be given.

Author's reply: The profile of δD-CH₄ is now discussed in more detail in the revised manuscript **(lines 424-427)**.

Referee's comment: L 84-85: Vivianite was found also in Lake Kinneret (Sivan et al., 2011), it can support your finding and related processes.

Author's reply: We have added this additional reference in the text **(line 86)**.

Referee's comment: L 92-93: Also propose the other option for Fe reduction.

Author's reply: Reactivation of more crystalline Fe oxides by methanogens has been added as an additional option (see comment above).

Referee's comment: L 141-142: See comment regarding this method above.

Author's reply: We have revised these lines according to the comment above.

Referee's comment: L. 151: I assume the auto analyzer was based on IR. How did you remove of the sulfide?

Author's reply: Samples for HPO_4^{2-} , DIC and HS^- were analyzed colorimetrically on two separate QuAatro (SEAL Analytical, Germany) auto-analyzers in thermo-stated containers. HPO_4^{2-} was measured at 880 nm after the formation of molybdophosphate-complexes (Murphy and Riley, 1962; *Anal. Chim. Acta*). Samples for DIC were acidified online after being oxidized by H_2O_2 and analyzed as described by Stoll et al. (2001; *Anal. Chem.*). The sulfide was trapped with NaOH and analyzed using the methylene blue method as described by Grasshof (1969; *Woods Hole Oceanographic Institute*). We have now added these details in the manuscript **(lines 157-162)**.

Referee's comment: L. 236-242: Clarify and explain this part in more details.

Author's reply: We have expanded this paragraph in the revised manuscript **(lines 252-257)**.

Referee's comment: L. 288: Show how you calculated to this saturation value and under which salinity conditions. Mark this value on the figures of methane too.

Author's reply: We have provided information on how this saturation concentration was derived **(lines 311-312)** and, as suggested by the referee, we have indicated the saturation concentration of CH_4 under atmospheric conditions in the Figures **(see Figs. 3, 4 and S5)**.

Referee's comment: Add the bottom water values on the porewater profiles

Author's reply: The bottom water values are already given in the pore water profiles (depth of 0 cm).

Referee's comment: L 297: Change the sentence to a more precise one.

Author's reply: This sentence has been improved in the revised version **(lines 320-322)**.

Referee's comment: L. 381: Explain the other 91% based on the profile (see main comment).

Author's reply: We have added the explanation in the revised manuscript **(lines 383-392)**.

Referee's comment: L 445-451: See the main comment regarding organoclastic Fe reduction.

Author's reply: We have expanded this section and now discuss why we assumed Fe-AOM as the only Fe reduction pathway in the model (also see comments to referee # 2) **(lines 496-499 and 247-251)**.

Referee's comment: L. 566-568: You don't need this trivial sentence, your work is good and nice enough without it.

Author's reply: We thank the referee for the compliment, but prefer to keep this sentence. In our opinion, it is important to include this statement because such diagenetic redistributions are often not considered in paleoceanographic studies.

Referee's comment: Fig. 3: No sulfate measurements in the sapropel depths ? Add saturation of methane. What could be the reaction precipitating phosphate in the upper 300 cm (hydroxyl-apatite)?

Author's reply: Unfortunately, the pore water samples for sulfate measurements in the sapropel depths were lost prior to analysis. We now provide information about the CH₄ saturation concentration in the revised version (**see Figs. 3, 4 and S5**). We suggest that the removal of dissolved phosphate in the upper 300 cm of sediment is due to authigenic apatite formation as observed previously in sediments of the Black Sea (Dijkstra et al. 2014; *PlosONE*) and have added this information to the revised manuscript (**lines 576-578**).

Referee's comment: Fig. 4: Again with the saturation of methane.

Author's reply: See comment above.

Referee's comment: L 339: Start a new subchapter.

Author's reply: We have added a subchapter for the rates and temporal evolution (**line 372**).

Referee # 2 (anonymous)

Referee's comment: This study addresses the diagenetic implications of anaerobic methane oxidation in Black Sea sediments where marine deposits overlie a freshwater facies into which a sulfate front is advancing. High-resolution geochemical profiles of dissolved and solid species are presented from two adjacent sites, and the profiles are simulated in a complex non-steady-state diagenetic model that derives rates of the relevant processes. The subject is interesting, obviously relevant to Biogeosciences, and the results and conclusions presented here are novel and add substantially to our understanding of sediment biogeochemistry and diagenesis. The text is well written, clear, and concise, the data is of good quality, and the conclusions are generally justified by the data and modelling. The authors particularly deserve credit for clearly distinguishing model results from reality. My main concern with the paper is that I miss a deeper analysis and discussion of the extent to which the modelling results are forced by the formulation and parameterization of the model. This could involve a sensitivity analysis or testing of alternative scenarios. Additionally, some aspects of the model results and formulation require clarification.

Author's reply: We thank the referee for the compliment. We reply to the comments below and have revised the manuscript accordingly (i.e. we have included a sensitivity analysis in the Supplementary Information and have clarified our model formulation and the corresponding results further).

Referee's comment: It is particularly the conclusions concerning sulfate- and iron-coupled AOM that require attention. The occurrence of Fe-AOM appears to be forced by the exclusion of organoclastic Fe reduction from the model, although there is plenty of evidence that organotrophic microbes can reduce crystalline Fe oxides, and there is no evidence that organotrophic Fe reduction cannot co-occur with methanogenesis if Fe reduction is limited by the availability/reactivity of iron oxides.

Author's reply: We thank the referee for the positive remarks. We acknowledge that the reason for the exclusion of organoclastic Fe reduction at depth in the sediment requires a more detailed explanation. The reason for this assumption was that we wished to test how important Fe-AOM could be for the CH₄ cycle, assuming that all the Fe reduction at depth would be exclusively due to Fe-AOM. We agree with the referee that organoclastic Fe reduction also provides a possible Fe reduction pathway and also state this in the original manuscript (see, for example lines 31-33, 476-478 and 559-560). In the revised manuscript, we have clarified our assumption for Fe-AOM and corresponding model results and formulation (**lines 496-499 and 247-251**).

Referee's comment: Furthermore, it seems that partitioning of AOM must be sensitive to the parameterization of the pathways, which therefore needs to be discussed.

Author's reply: The sensitivity of the AOM partitioning is now discussed in the caption of **Supplementary Fig. S2**.

Referee's comment: 22-23+89-90: The finding that sulfate-AOM enhances the sulfide flux is not novel according to lines 72-75.

Author's reply: We agree with the referee, and have rephrased the text so that it is clear that we are not implying that this is a novel finding (**lines 22 and 92-93**).

Referee's comment: 289-96: Just a comment: The difference in the two methane profiles is strange and it is difficult to understand how degassing would have caused a proportional decrease in methane in the zone above the zone of saturation. Nonetheless, I agree that it is the most likely explanation given the similarity of all other profiles, including the methane isotopes. I suggest rephrasing 293-294 to clarify which methane data this applies to.

Author's reply: We elaborate on the degassing of CH₄ and clarify our conclusions in the revised manuscript (**lines 311-317**).

Referee's comment: 339-41+Fig 6: I don't understand the very high rates of sulfate reduction and methanogenesis in the sapropel, and the model doesn't seem to fit the data well here. Albeit noisy, the measured H₂S profile seems straight or even concave in this region, and the same clearly goes for DIC, whereas the model profiles are convex, which suggests that the model overestimates the rates substantially. Although this zone is not of primary interest in this study, an overestimation of rates and product concentrations results in a shallower gradient from unit II to the SMTZ and therefore in lower sulfate-AOM rates, so the fit here still influences the central conclusions.

Author's reply: The rates of sulfate reduction and methanogenesis were corrected (**lines 363-367; see also Table 6 and Fig. 6**) and are now significantly smaller (see comment below). We have also improved the model fits for H₂S and DIC in the marine deposits (**see Fig. 3**). The fit still is not perfect, but the small offset does not impact our conclusions.

Referee's comment: Fig. 6, further+ Fig. 3: There seems to be an error in the H₂S production panel in Fig. 6 as H₂S production from sulfate reduction is only a fraction of the sulfate reduction rate? Shouldn't these be 1:1 as is the case for sulfate-AOM and sulfide production from sulfate AOM? Also, what happens to methane produced in unit II? The methane profile appears flat, yet only a fraction of the production is consumed by AOM. Please provide blow-ups of modelled methane in the upper 2 m and of sulfate below the SMTZ in Fig. 3.

Author's reply: We thank the referee for pointing out these inconsistencies. The rate plots of Fig. 6 were not normalized to the same volume, meaning that the SO₄ reduction rate, CH₄ production and S₀ disproportionation should be multiplied by the solid volume fraction of the sediment, while rates of SO₄-AOM and Fe-AOM should be multiplied by the sediment porosity. In addition, only 0.5 mole of CH₄ are produced per mole of organic matter during methanogenesis (see reaction R5 in Table 3). We have changed the unit conversion in the plotting, as well as the mass balance and have revised **Fig. 6 and Table 6** accordingly.

Referee's comment: 391-5: This is the only real flaw in the paper. The Rayleigh function applies to closed systems and should never be used in open systems such as this one, where diffusion affects the relative distribution of the isotopes. Accurate enrichment factors can only be derived through modelling (e.g., Alperin et al. 1988). The closed-system approach will underestimate enrichment factors substantially in most cases, and likely explains the low value derived here. This problem was described decades ago (e.g., Jørgensen 1979, GCA 43:363).

Author's reply: We thank the referee for this critical remark. We agree that modeling of the methane isotopes would result in a more reliable estimation of the enrichment factors. However, the determination of isotopic fractionation was not the main aim of this study. In addition, considering that diffusion fractionation is likely minor compared to the fractionation associated with oxidation (e.g. Happell et al., 1995; *Limnol. Oceanogr.*; Chanton, 2005; *Org. Geochem*) and that diffusion might be slower than oxidation in our settings, it could be argued that we may be looking at a quasi-closed environment. We have now clarified the limitation of our approach in the revised manuscript (**lines 431-437**).

Referee's comment: 401: I think some of these studies observed sulfate reduction and did not only postulate it?

Author's reply: We agree with the referee and have changed this in the revised manuscript (**line 443**).

Referee's comment: 442-3: Under which conditions, if any, within a realistic parameter space or with an alternative set of reactions, would a cryptic sulfur cycle be able to explain the accumulation of Fe²⁺?

Author's reply: We now elaborate on this in the revised manuscript (**lines 483-485**).

Referee's comment: 450-5: The references listed here suggest that AOM may be coupled to Fe reduction, but here you really use them to support the assumption that Fe reduction can be coupled to AOM rather than to organoclastic Fe reduction – Is there any support for that in any of those references? As stated in l. 463, organoclastic Fe reduction is clearly limited at these depths, but that doesn't mean that it is absent. Furthermore l. 474-6 seems to suggest organoclastic Fe reduction anyway, even if it is by archaea? But what special skills do these organisms have that would enable them to reactivate Fe oxides?

Author's reply: We acknowledge that lines 450-5 in the original manuscript could be formulated better. The existing literature cited here indicates that Fe reduction could be coupled to CH₄ oxidation in aquatic sediments. The aim of this study was thus to evaluate whether the geochemical profiles could be reproduced assuming that all Fe reduction at depth would be coupled to Fe-AOM and to show the potential impact of Fe-AOM on the CH₄ cycle. We are not claiming that Fe-AOM is more likely than organoclastic Fe reduction, but rather show that Fe-AOM represents a plausible mechanism for the deep Fe reduction. We have now clarified this in

the revised manuscript (**lines 496-499 and 247-251**). To our understanding, the underlying mechanisms of the reactivation of Fe oxides by methanogens as described by Sivan et al. (2016; *Geobiology*) remain enigmatic.

Referee's comment: 489-93: It seems trivial that in situ rates under the given conditions are low compared to lab-based rates. What is the observational basis for the parameterization of the reaction?

Author's reply: The Fe-AOM reaction was implemented according to Beal et al. (2009; *Science*) and the rates were derived by fitting the modeled pore water and solid phase profiles with the observations as explained in the text (lines 239-241). In our view, it is not trivial to mention the difference in rates calculated here and observed in laboratory experiments in other settings. It illustrates that it may be difficult to perform laboratory incubations of Black Sea sediments to study Fe-AOM.

Referee's comment: 494-5: How sensitive is the sulfate/Fe-AOM partitioning to the parameterization?

Author's reply: We have performed an appropriate model sensitivity analysis in the revised manuscript and discuss its sensitivity in the caption of **Supplementary Fig. S2**.

Referee's comment: Table 3, R6+16: I understand that you need a sink for H₂, but why is it only methanogenesis and not, at least sulfate reduction? This will lead to overestimation of methanogenesis in the sulfate zone.

Author's reply: The referee is kindly referred to Table 2, where it becomes evident that H₂ is not explicitly modeled in this study.

Referee's comment: Table 4: R19+ R20 are biological processes and as such might obey biological (saturation) kinetics? These are key reactions in the paper and the observational basis for the kinetic expressions, and their impact on the conclusions should be discussed.

Author's reply: The bimolecular rate equation expression for AOM applied in this study is the most frequently used AOM parameterization in reactive transport models (Regnier et al., 2011; *Earth-Science Reviews*). We followed the bimolecular approach because of the high uncertainty in half-saturation constants, in particular for the putative Fe-AOM pathway. For a detailed discussion about AOM parameterization, the referee is kindly referred to the study by Regnier et al. (2011; *Earth-Science Reviews*). We now justify our choice for the AOM parameterization in the revised manuscript (**lines 265-268**).

Table 6 + Fig 6: The labelling of the two kinds of methanogenesis is misleading. The light isotopic composition of methane implies that it is formed mainly through CO₂ reduction rather than acetoclastic methanogenesis, i.e. that "Methanogenesis (OM)" is mainly CO₂-based. "Methanogenesis (DIC)" is really a peculiarity of the model and completely and uniquely linked

to pyrite formation, so “Methanogenesis (FeS₂)” would be more appropriate (but see also comment to Table 3 above).

Author’s reply: We agree with referee that reaction R6 in Table 3 and the labeling in Table 6 and Fig. 6 are difficult to understand and have improved it in the revised version (see the caption of Table 3). Furthermore, the two CH₄ pathways are now summed together in Table 6 and Fig. 6.

Referee’s comment: Fig. 7: Consider a colour version here. The darkest shading on the scale bars always appears darker than the darkest part of the figures. Because the shading varies so little from min. to max. it is very difficult to extract quantitative information.

Author’s reply: We have changed Fig. 7 to a color version.

Referee # 3 (W.-L. Hong)

Referee's comment: Overall comments In the paper, Egger et al. present very comprehensive porewater and sediment geochemical data to discuss the cycles of C, S, Fe, and P in sediments that are unique in the sense of their depositional sequence and history. The authors collectively discuss the data with a rather complicated model, which is understandable due to the complexity of the system they work with. The paper is well-written and structured. The authors' attempt to elucidate the mass balance of several elements in this environment provide valuable insights to the coupling of these elements and the complexity of it. In general, the conclusions are convincing and well support by their data and modeling. As also a user of such transport-reaction models (Hong et al., 2014a&b; Torres et al., 2015; Hong et al., 2016), my major concern of the paper will be on the assumptions and setup of the model as well as several interpretations the authors made based on the model results. In conclusion, I think this is a very nice piece of work considering all the data and modeling work.

Author's reply: We thank the referee for the compliment. We reply to the comments below and have revised the manuscript accordingly.

Referee's comment: Major comments Modeling numerical issue: In conventional models for transportreaction models, advection (i.e. sediment burial) often inevitably results in numerical dispersion, concentration will decrease as time progresses with burial even without any reaction. This effect will be especially obvious when using high advection rate (burial rate), large time discretization, and a long modeling time. I've done some tests before (Hong et al., 2016 accepted by limnology and oceanography) by simulating time progression of a profile with sharp concentration change. After 140 years of simulation, the concentration is 20% reduced compared to the value it should have (see the attached file for this comparison). As for the sharp increase of OM content in your environment, you will inevitably encounter this numerical issue. I urge the authors to run some simulations with only burial (no diffusion and other reactions), and see how your sediment and porewater profiles will progress.

Author's reply: We thank the referee for sharing his experience with us. The ReacTran package applied in this study (see line 285) accounts for numerical dispersion using total variation diminishing (TVD) slope limiters. A description of the ReacTran package can be found at: <https://cran.r-project.org/web/packages/ReacTran/ReacTran.pdf>

Referee's comment: I also wonder what is the consequence to accelerate your model. The price of numerical issues will be greater when you accelerate it by using larger time steps and/or faster rates. It is almost no way to have a model that is both efficient and accurate. There is always a sacrifice.

Author's reply: We could not find any indication that the model acceleration impacts the conclusions presented in this study. A higher sedimentation rate in the lake phase, however, largely improves the model efficiency as it significantly reduces the computing time.

Referee's comment: The other potential numerical issue I want to point out for the authors is the convergence of the model results. You have to make sure you use temporal and spatial steps small enough so that the results are stable. This can be done by running the model several times (the same reactions and setup) with smaller time/space discretization for each run. Chose the smallest discretization that your model results stop changing.

Author's reply: We used this approach in this study (i.e. we ran the model using various time and space discretizations). The model presented here thus reflects the smallest discretization for which the model results stop changing.

Referee's comment: Conflict between observations and model results: In a few places in the paper, the authors didn't explain clearly the conflict between observations and model results. One example is the choice of chloride changes with time. The authors used a very different evolution pattern from what literature suggested because it provides a better fit of their chloride concentration. However, the time scale adopted by the authors (100yrs) is an order smaller than what is suggested in the literature (2000yrs). The authors provide no explanation about such difference. I envision that if the author use constant chloride from 2000yrs BP until now and increase fluid advection rate (larger u), they might be able to fit the profile. I think the authors should explain better why choosing such condition.

Author's reply: We extended the total length of the model domain to 3000 cm (see lines 280-282), which allowed us to modify our salinization scenario to make it much more similar to that of Soulet et al. (2010) (**lines 293-298**).

Referee's comment: The other example is from line 369 to 371. The authors claimed the SR rates they estimated from the model in zone I & II are more correct the estimation from porewater profiles. This statement raises the question that, then how do you know the SR rate you estimated from these two zones are accurate since you have no data to support you.

Author's reply: Sulfate reduction rates derived from pore water profiles represent net sulfate consumption, while rates derived from radiotracer injection and diagenetic modeling reveal total sulfate turnover in the sediment, i.e. gross sulfate reduction rates (e.g. Jørgensen (1978; *Geomicrobiol. J.*) and Jørgensen et al. (2001; *Deep Sea Res. Part I*)). Thus, modeled rates are generally higher than rates estimated from pore water profiles. We have clarified this in the revised manuscript (**lines 402-404**). The referee is further kindly referred to lines 394-395 where we provide references to studies that have measured sulfate reduction rates in Black Sea sediments, which compare well with our model results.

Referee's comment: Very high methanogenesis rate in sulfate reduction zone: In fig 6, there are two peaks of methane production (one in bottom water or first cm of sediment? While the other in zone II). My questions are two: 1) It is apparent that this methanogenesis is from OM decomposition. However, methanogenesis should be suppressed when the sulfate content is high, as in the case of zone II. I understand that although methanogenesis is inhibited by sulfate

content (E5 & E6 in Table 4), model can still produce very high ME rate when there is ultrahigh OM content. However, a model is a model, do you have any prove such high methanogenesis from your zone I and II. Considering the CH₄ production rate and SO₄-AOM rate from Fig.6. you should see either high methane or light d13C of methane in zone I and II if the rate is this high. I however don't quite see those from your profiles.

Author's reply: The CH₄ production rate depicted in the original Fig. 6 is not correct, as it should be multiplied with the solid volume fraction of the sediment (increases from ~ 0.05 at the sediment surface to ~ 0.39 at depth) and divided by a factor of two (only 0.5 mole of CH₄ are produced per mole of organic matter during methanogenesis; see reaction R5 in Table 3; also see response to referee #2). Actual modeled rates of CH₄ production are thus < 30 pmol cm⁻³ d⁻¹ in the marine deposits, which is an order of magnitude lower than modeled SO₄-AOM rates. Our modeled CH₄ production rates in the surface sediments (~ 7 pmol CH₄ cm⁻³ d⁻¹) are still significantly lower than net rates of methanogenesis measured in surface sediments of the Peruvian margin of up to ~ 1 nmol cm⁻³ d⁻¹ in the sulfate reduction zone, for example (Maltby et al., 2016; *Biogeosciences*).

Referee's comment: 2) Back to fig6, your rates do not seem to balance. The highest CH₄ production rate approaches 300 pmol/cm³/d which only stimulates an AOM rate less than maybe 20 pmol/cm³/d. If there is more production than consumption, isn't that you will methane accumulates in the porewater (i.e., high methane from that depth in the sediments). SR rate is over 2000 pmol/cm³/d in this section but sulfide production is only 300 pmol/cm³/d. where is the rest of sulfide production?

Author's reply: We thank the referee for pointing out these inconsistencies. There has been an error in the plotting of the rates (see also answer to referee #2). The rate plots of Fig. 6 were not normalized to the same volume, meaning that the SO₄ reduction rate, CH₄ production and S₀ disproportionation should be multiplied by the solid volume fraction of the sediment, while rates of SO₄-AOM and Fe-AOM should be multiplied by the sediment porosity. In addition, only 0.5 mole of CH₄ are produced per mole of organic matter during methanogenesis (see reaction R5 in Table 3). We have corrected these errors in the revised manuscript (see Table 6 and Fig. 6).

Referee's comment: The very complicated model: The authors use a rather complicated model in this study by choosing many reactions that are not totally necessary. For example, the authors choose to include aerobic processes (R1, R7-R12) and nitrate reduction (R2) even though there is no constraints on O₂ and nitrate content in the porewater. I would also doubt the importance of these reactions due to the anoxic bottom water in Black Sea. The authors chose not to include Mn reduction due to its low content, which is fine with me, but decide to include all other processes that cannot be constrained? That is an odd decision to me. By excluding these unnecessary reactions, the authors can also improve the efficiency of the model.

Author's reply: Oxic mineralization and nitrate reduction were implemented because of the oxic Black Sea lake phase. Bottom water concentrations of oxygen and nitrate for the Lake phase were taken from Reed et al. (2011; *GCA*). We agree with the referee that nitrate reduction plays only a minor role (also during the oxic Lake phase), but prefer to keep the reaction in the model, as removing it does not significantly improve the model efficiency.

Referee's comment: I also wonder, with all the reactions assigned in the model, do the authors have enough constraints? I believe the answer should be close to yes as the authors have many data to support the model (which is very nice). I would urge the authors to spare a section in the text discussing the constraints for the model. To me, this is an extremely important but often ignored aspect in papers like this. I have done some initial analyses based on the reaction network in Table 3. For example, for Fe²⁺, the authors have R3, R9, R10, R13, R14, and R20 for sources, and R8, R15, R23, and R24 for sinks. Some source and sink terms may be constrained by the data of iron mineral speciation. When the same analyses being applied on HS in porewater, it seems like the abundance of different Fe-S minerals also depend on the source and sink terms of HS. A table such as tab6 but with more species included may be useful for such discussion.

Author's reply: We kindly refer the referee to lines 239-241 and Table 5 where we describe the parameter constraints. We have now added a table with the mass balance for each species in the Supplementary Information (**see Supplementary Table S2**).

Referee's comment: One last comment on the complicated model, how does the model describe pH, which should be very important determining the type of dissolved sulfide and DIC. I don't see reactions such as H₂S becomes HS-+H⁺ in Tab3 which describe the buffer capability of HS species (need same reactions for carbonate systems). Although there is usually no good constraint on pH, it's good to make sure pH falls in the right range especially when including pH-sensitive reactions.

Author's reply: The model does not include pH, because it does not capture the precise underlying reaction mechanisms. Furthermore, we do not have pH data to compare the model results to. Adding pH would be a separate study in itself.

Referee's comment: Minor comments Line 151: Please specify how you measure sulfide, phosphate, and DIC onboard.

Author's reply: We have now added this information in the revised manuscript (**lines 157-162**).

Referee's comment: Line 211: why 20 meters? You should mark you explain this in the supplemental material.

Author's reply: The referee is kindly referred to lines 279-280 and Supplementary Fig. S6. Note that it has changed to 30 m in the revised manuscript (see above).

Line 255: is zero gradient a good assumption for methane? How do you know there is no deeper source of methane?

Author's reply: We have no information about a potential deep source of CH₄ at our study site. However, the good fit between the modeled and measured ammonium profile (Fig. 3) indicates that it is likely that most of the CH₄ is produced within the model domain. We therefore think that a zero gradient assumption is a reasonable assumption for CH₄.

Referee's comment: Line 289 to 293: You have same ammonium but higher methane in site 4 and 5. Of course more severe degassing during core recovery in site 4 can be one explanation, but maybe there is more methane input from site 5 from greater depth. This echoes back my previous comment: is zero gradient really a good assumption for methane?

Author's reply: If the difference in the CH₄ profiles between site 4 and 5 would be due to more CH₄ input from greater depth at site 5, it would imply that the measured concentrations at site 4 represent actual in-situ concentrations of pore water CH₄. However, we were not able to reproduce the observed ammonium profiles with such low rates of methanogenesis at depth. In contrast, our model suggests that in order to have sufficient pore water ammonium, CH₄ concentrations should be significantly higher than the measured concentrations at both sites. The high CH₄ concentrations derived from the model are also consistent with our observations of massive CH₄ degassing during coring and with previous observations in the western Black Sea shelf (Jørgensen et al., 2001; *Deep Sea Res. Part I*). We conclude that the ammonium profiles indicate that most of the CH₄ is produced within the model domain, rather than from greater depths, thus supporting our zero gradient assumption.

Referee's comment: Line 304: How do you know the isotopic signature of methane is not affected by degassing?

Author's reply: We base this conclusion on the smooth pore water profiles of $\delta^{13}\text{C-CH}_4$ and $\delta\text{D-CH}_4$ (see Fig. 4). To date, little is known about potential isotopic fractionation during degassing. However, it is thought that fast degassing is unlikely to result in major isotopic fractionation, as all CH₄ isotopes are lost simultaneously. We now clarify this in the revised manuscript (**line 328**).

Referee's comment: Line 533: Isn't that this will be capture in your orgP analyses?

Author's reply: Mineral formation in microbial cells is not included in the model. Inclusions of Fe-P minerals initially formed in bacteria could be dissolved in the CDB step of the SEDEX extraction (Dijkstra et al., 2014, PLoS ONE).

Referee's comment: Line 827: Do you have any constrain on C/P ratio? Maybe this explains why the fitting on porewater phosphate profile is not as good?

Author's reply: The C/P ratio observed in the sedimentary record does not necessarily directly relate to the initial C/P ratio of the organic matter deposited on the seafloor due to the preferential

regeneration of phosphorus from organic matter during anaerobic degradation (e.g. Ingall et al., 1993; *GCA*). It is thus of limited use as a constraint in this study.

Referee's comment: Salinity/chloride: In many places of the paper, the authors mixed the term salinity and chloride concentration (e.g., line268-282). Of course these two properties are usually linear dependent on each other but they are fundamentally different and may correlate with each other very differently when Black Sea was more of a "lake" or a "Sea". I suggest the authors to use chloride concentration throughout the paper or explain how they convert salinity to chloride concentration.

Author's reply: We have followed the referee's suggestion and explain how salinity is converted to chloride concentrations in the revised manuscript (**lines 297-298 and Supplementary Table S1**).

Referee's comment: FigS3: What is going on with the very high alkalinity at very top? where dic concentration looks normal...

Author's reply: We thank the reviewer for pointing this out. After carefully checking the data, we have decided to omit them from the Supplementary Information due to uncertainty over data quality.

List of all relevant changes made in the manuscript

- Model sensitivity analysis to show the uncertainties associated with key processes (presented in the Supplementary Information, Figs S2 and S3)
- Model grid changed from constant to exponentially decreasing in order to speed up the sensitivity analyses (no effect found for model results)
- Revision of the salinization scenario to make it consistent with existing literature
- Providing information on how salinity was converted to Cl^- and SO_4^{2-}
- Clarification of model formulation and corresponding results
- Mass balance for each species in the Supplementary Information (Table S2)
- More detailed explanation why we assume Fe-AOM as the only Fe reduction pathway at depth in the model
- Clarification of pore water subsampling methods
- More detailed information about methane saturation concentration and degassing of methane (also indicated in Figs 3 and 4)
- Correction of the rates shown in Fig. 6 and corresponding revision of Table 6
- Discussion of the limitation of the Rayleigh function to estimate fractionation factors in our study
- Showing the potential release of dissolved Fe^{2+} via cryptic S cycling in our model
- Fig. 7 has changed to a color version
- More detailed discussion of sulfate and methane pore water profiles and corresponding fluxes of methane and sulfate to the SMTZ
- Reactivation of less reactive iron oxides highlighted as alternative iron reduction pathway

Anaerobic oxidation of methane alters sediment records of sulfur, iron and phosphorus in the Black Sea

Matthias Egger¹, Peter Kraal¹, Tom Jilbert^{1,2}, Fatimah Sulu-Gambari¹, Célia J. Sapart^{3,4}, Thomas Röckmann³ and Caroline P. Slomp¹

¹Department of Earth Sciences – Geochemistry, Faculty of Geosciences, Utrecht University, P.O. Box 80021, 3508 TA, Utrecht, The Netherlands

²Now at: Department of Environmental Sciences, Faculty of Biological and Environmental Sciences, University of Helsinki, P.O. Box 65 (Viikinkaari 2a), 00014 Helsinki, Finland

³Institute for Marine and Atmospheric Research Utrecht (IMAU), Utrecht University, Princetonplein 5, 3584 CC Utrecht, The Netherlands

⁴Laboratoire de Glaciologie, Université Libre de Bruxelles, Belgium

Correspondence to: Matthias Egger (m.j.egger@uu.nl)

Abstract. The surface sediments in the Black Sea are underlain by extensive deposits of iron (Fe) oxide-rich lake sediments that were deposited prior to the inflow of marine Mediterranean Sea waters ca. 9000 years ago. The subsequent downward diffusion of marine sulfate into the methane-bearing lake sediments has led to a multitude of diagenetic reactions in the sulfate-methane transition zone (SMTZ), including anaerobic oxidation of methane (AOM) with sulfate. While the sedimentary cycles of sulfur (S), methane and Fe in the SMTZ have been extensively studied, relatively little is known about the diagenetic alterations of the sediment record occurring below the SMTZ.

Here we combine detailed geochemical analyses of the sediment and pore water with multicomponent diagenetic modeling to study the diagenetic alterations below the SMTZ at two sites in the western Black Sea. We focus on the dynamics of Fe, S and phosphorus (P) and demonstrate that diagenesis has strongly overprinted the sedimentary burial records of these elements. **In line with previous studies in the Black Sea**, we show that sulfate-mediated AOM substantially enhances the downward diffusive flux of sulfide into the deep limnic deposits. During this downward sulfidization, Fe oxides, Fe carbonates and Fe phosphates (e.g. vivianite) are converted to sulfide phases, leading to an enrichment in solid phase S and the release of phosphate to the pore water. Below the sulfidization front, high concentrations of dissolved ferrous Fe (Fe^{2+}) lead to sequestration of downward diffusing phosphate as authigenic vivianite, resulting in a transient accumulation of total P directly below the sulfidization front.

Our model results further demonstrate that downward migrating sulfide becomes partly re-oxidized to sulfate due to reactions with oxidized Fe minerals, fueling a cryptic S cycle and thus stimulating slow rates of sulfate-driven AOM ($\sim 1 - 5 \text{ pmol cm}^{-3} \text{ d}^{-1}$) in the sulfate-depleted limnic deposits. However, this process is unlikely to explain the observed release of dissolved Fe^{2+} below the SMTZ. Instead, we suggest that besides organoclastic Fe oxide reduction **and reactivation of less reactive Fe oxides by methanogens**, AOM coupled to the reduction of Fe oxides may also provide a possible mechanism for the high concentrations of Fe^{2+} in the pore water at depth. Our results reveal that methane plays a key role in the diagenetic alterations of Fe, S and P records in Black Sea sediments. The downward sulfidization into the limnic deposits is enhanced through sulfate-driven AOM with sulfate and AOM with Fe oxides may provide a deep source of dissolved Fe^{2+} that drives the sequestration of P in vivianite below the sulfidization front.

39 Anaerobic oxidation of methane (AOM), a process initially regarded as a biogeochemical curiosity, functions as an
40 important sink for oceanic methane (CH₄) by consuming > 90 % of all CH₄ produced in marine sediments (Knittel
41 and Boetius, 2009; Reeburgh, 2007). Although recent studies indicate that the biological oxidation of CH₄ could be
42 coupled to various additional electron acceptors such as nitrate and nitrite (Ettwig et al., 2010; Raghoebarsing et al.,
43 2006) as well as metal oxides (Beal et al., 2009; Egger et al., 2015b; Riedinger et al., 2014; Scheller et al., 2016;
44 Segarra et al., 2013; Sivan et al., 2011), sulfate (SO₄²⁻) is commonly thought to be the dominant electron acceptor in
45 anoxic marine systems (Knittel and Boetius, 2009; Reeburgh, 2007).

46 Nevertheless, a coupling between anaerobic CH₄ oxidation and iron (Fe) oxide reduction (Fe-AOM) could have a
47 significant impact on sedimentary Fe cycling and related processes such as phosphorus (P) diagenesis, because of the
48 8:1 Fe-CH₄ stoichiometry of the reaction (Beal et al., 2009; Egger et al., 2015a; Rooze et al., 2016). Environmental
49 conditions that favor Fe-AOM in marine systems are still poorly understood. The required co-occurrence of pore
50 water CH₄ and abundant reducible Fe oxides suggests that Fe-AOM may occur in sediments that receive a relatively
51 high input of Fe oxides compared to the in-situ production of sulfide, which could allow a portion of Fe oxides to
52 escape the conversion to authigenic Fe sulfides and to remain preserved in the methanogenic sediments below the
53 zone of SO₄²⁻ reduction (Egger et al., 2015b; Riedinger et al., 2014; Rooze et al., 2016). In addition, perturbations
54 inducing transient diagenesis such as anthropogenic eutrophication or climate change may also create diagenetic
55 environments that are likely favorable for Fe-AOM, as they provide a mechanism for the burial of Fe oxide-rich
56 deposits below sulfidic sediment layers (Egger et al., 2015b; Riedinger et al., 2014).

57 The Black Sea represents a good example of a sedimentary system in which transient diagenesis associated with
58 postglacial sea-level rise has led to the accumulation of sulfidic sediments above Fe oxide-rich deposits. Here, the
59 establishment of a connection to the Mediterranean Sea through the shallow Bosphorus around 9000 years ago
60 (Degens and Ross, 1974; Soulet et al., 2011) led to the inflow of marine waters into a freshwater basin, resulting in
61 permanent salinity/density stratification and in the development of euxinic conditions (i.e. free dissolved sulfide
62 present in the bottom water), making the current Black Sea the largest permanently anoxic basin on Earth.

63 In the absence of oxygen and metal oxides, SO₄²⁻ reduction is the dominant benthic mineralization process of organic
64 matter in Black Sea surface sediments below the chemocline (~ 100 m depth) (Jørgensen et al., 2001; Thamdrup et
65 al., 2000). At present, SO₄²⁻ penetrates through the modern coccolith ooze (Unit I) and the marine sapropel (Unit II)
66 sediments and a few meters into the Upper Pleistocene freshwater deposits (Unit III) (Arthur and Dean, 1998;
67 Degens and Ross, 1974; Jørgensen et al., 2004). Below the SO₄²⁻-bearing zone, methanogenesis takes over as the
68 dominant process of organic matter degradation, resulting in the buildup of CH₄ in the pore water at depth.

69 Interactions between the cycles of sulfur (S) and CH₄ in Black Sea sediments have been extensively studied during
70 recent years (Holmkvist et al., 2011b; Jørgensen et al., 2001, 2004; Knab et al., 2009; Leloup et al., 2007) and AOM
71 coupled to SO₄²⁻ reduction (SO₄-AOM) was found to account for an estimated 7-18 % of total SO₄²⁻ reduction in
72 these sediments (Jørgensen et al., 2001). The production of sulfide in the sulfate-methane transition zone (SMTZ) as
73 a result of SO₄-AOM represents the main source of pore water sulfide at depth in the sediment. This intensified
74 production of sulfide drives an enhanced downward diffusive flux of sulfide into the deep limnic deposits of Unit III,

75 forming a distinct diagenetic sulfidization front recognized as a black band or a series of bands owing to the
76 conversion of Fe oxides to Fe sulfides (Berner, 1974; Jørgensen et al., 2004; Neretin et al., 2004).
77 At present, the impact of the downward-migrating sulfidization front on sedimentary P, a key nutrient for marine
78 phytoplankton, and the potential role of Fe-mediated AOM in the deep limnic deposits remain largely unknown. A
79 buildup of ferrous Fe (Fe^{2+}) in the pore water at depth as found in previous studies (Holmkvist et al., 2011b;
80 Jørgensen et al., 2004; Knab et al., 2009), could indicate ongoing Fe reduction in the CH_4 -bearing deep limnic
81 sediments and thus a potential coupling between AOM and Fe oxide reduction. The sediment records investigated up
82 to now, however, do not extend deep enough to allow the sedimentary cycling of Fe and related biogeochemical
83 processes below the sulfidization front to be investigated. In particular, the presence of abundant dissolved Fe^{2+}
84 combined with a potential release of pore water phosphate (HPO_4^{2-}) during reductive dissolution of Fe oxides may be
85 conducive to the formation of reduced Fe(II)-P minerals such as vivianite ($\text{Fe}_3(\text{PO})_4 \cdot 8\text{H}_2\text{O}$) below the sulfidization
86 front (Egger et al., 2015a; Hsu et al., 2014; März et al., 2008; Sivan et al., 2011). Post-depositional diagenetic
87 alterations as a result of downward sulfidization could therefore overprint burial records of P in the Upper
88 Pleistocene deposits.

89 In this study, we combine detailed geochemical analyses of the sediment and pore water with multicomponent
90 diagenetic modeling to study the diagenetic alterations below the lake-marine transition at two sites in the western
91 Black Sea. Focusing on the dynamics of S, Fe and P, we demonstrate that AOM coupled to SO_4^{2-} reduction enhances
92 the downward sulfidization and associated dissolution of Fe oxides, Fe carbonates and vivianite, supporting earlier
93 findings of an SO_4 -AOM enhanced downward sulfidization in Black Sea sediments (Jørgensen et al., 2001). Below
94 the sulfidization front, downward diffusing HPO_4^{2-} precipitates as vivianite by reaction with the abundant dissolved
95 Fe^{2+} . We propose that organoclastic Fe oxide reduction, reactivation of less reactive Fe oxides by methanogens
96 (Sivan et al., 2016) and/or AOM coupled to the reduction of Fe oxides are the key processes explaining the high
97 concentrations of dissolved Fe^{2+} at depth in the sediment. Trends in total S and P with depth are significantly altered
98 by the above-mentioned reactions, highlighting that diagenesis may strongly overprint burial records of these
99 elements below a lake-marine transition.

100 2 Materials and methods

101 2.1 Sample collection

102 2.1.1 Gravity core sampling

103 Sediment samples were taken at two slope sites in the western Black Sea during a cruise in June 2013 with R/V
104 Pelagia. Gravity cores containing ~ 7 m of sediment were collected at sites 4 ($43^\circ 40.6'$ N, $30^\circ 7.5'$ E; 377 meters
105 below sea surface (mbss)) and 5 ($43^\circ 42.6'$ N, $30^\circ 6.1'$ E; 178 mbss) (Fig. 1), both situated below the current
106 chemocline (~ 100 m water depth). The core liners were pre-drilled with 2 cm diameter holes in two rows of 10 cm
107 resolution on opposing sides of the tube, offset by 5 cm and taped prior to coring. Upon recovery, the liners were cut
108 into 1 m sections, transferred to a temperature-controlled container set at in-situ bottom water temperature (11 °C)

109 and secured vertically. Subsequently, the taped holes were cut open and a cut-off syringe was inserted horizontally
110 directly after opening each hole.

111 From one series of holes, 10 mL of wet sediment was extracted at 20 cm resolution and immediately transferred into
112 a 65 mL glass bottle filled with saturated NaCl solution for CH₄ analysis. The NaCl solution was topped up after
113 addition of the sample, ensuring that no air bubbles remained. Each bottle was sealed with a black rubber stopper and
114 a screw cap and was subsequently stored upside-down at room temperature. From the second series of holes, 20 mL
115 sediment was extracted at 20 cm resolution, sealed with parafilm that was tightly closed with an elastic band, and
116 directly inserted into a nitrogen (N₂)-purged glove box. Subsequently, the sediment was transferred into a 50 mL
117 centrifuge tube and centrifuged (4500 rpm; 30 min). The supernatant from each centrifuged sample was filtered
118 through 0.45 µm pore size disposable filters via 20 mL plastic syringes in the glove box and collected in 15 mL
119 centrifuge tubes. The sediment fraction was stored frozen (-20 °C) for solid phase analysis. Filtered pore water
120 samples were sub-sampled under N₂ for analysis of dissolved HPO₄²⁻, ammonium (NH₄⁺), dissolved inorganic
121 carbon (DIC), Fe, manganese (Mn), SO₄²⁻ and sulfide (ΣH₂S = H₂S + HS⁻) (see section 2.2) Additional samples of 10
122 mL of sediment were collected at approximately 50 cm resolution and transferred into pre-weighed 15 mL glass vials
123 to determine porosity from gravimetric water loss.

124 **2.1.2 Multicore sampling**

125 To sample the surface sediment, sediment cores (30-60 cm of sediment and at least 10 cm of overlying water) were
126 recovered using an octopus multicorer (core diameter 10 cm). After recovery, the cores were stoppered at the base
127 and at the top and immediately transported to a temperature-controlled container (11 °C). One multicore from each
128 cast was pre-drilled with 2 cm diameter holes in two rows at 10 cm resolution on opposing sides of the tube, offset
129 by 5 cm, and taped prior to coring. These holes were sampled for CH₄ as described for the gravity cores. Another
130 core was directly inserted into a N₂-purged glove box through an airtight hole in the base. A bottom water sample
131 was collected using a 20 mL plastic syringe and the remaining bottom water was removed with a Tygon tube.
132 Subsequently, the core was sliced anoxically with decreasing resolution at depth, i.e. 0.5 cm resolution for the first 0-
133 2 cm, 1 cm resolution between 2-10 cm, 2 cm resolution between 10-20 cm and 4 cm resolution for the rest of the
134 core (> 20 cm). For each slice a sub-sample was placed in a pre-weighed 15 mL glass vial for water content and solid
135 phase analysis and stored under N₂ in airtight jars at -20 °C. A second sub-sample was transferred to a 50 mL
136 centrifuge tube and centrifuged (4500 rpm; 30 min). Both the supernatant water from each centrifuged sample and
137 the bottom water sample were subsequently processed as described for the gravity cores.

138 Visual alignment of the pore water profiles from the multicores with those of the gravity cores showed that the first ~
139 20 to 30 cm of sediment was lost during long coring. At site 5, the sediment in the multicore consisted of a gray and
140 homogeneous turbidite below 1.5 cm depth. The depth for the gravity core at site 5 was thus corrected for the loss of
141 the marine deposits, which were previously reported to be about 50 cm thick at a site in close proximity to site 5
142 (43°42.63' N, 30°6.12' E; 181 mbss) (Jørgensen et al., 2004)

143 2.2 Pore water subsampling

144 A sub-sample of 0.5 mL was immediately transferred into a glass vial containing 1.5 mL of 8 M NaOH solution for
145 analysis of dissolved sulfide. Sub-samples for total dissolved Fe and Mn, which are assumed to represent Fe(II) and
146 Mn(II), were acidified with 10 μ L 35 % suprapur HCl per mL of sub-sample. Note, however, that the dissolved (<
147 0.45 μ m) Fe and Mn pools likely consist of a mixture of truly dissolved (aqueous), as well as organically complexed,
148 colloidal and nanoparticulate Fe and Mn species (Raiswell and Canfield, 2012). Another 1 mL of pore water for
149 HPO_4^{2-} analysis was acidified with 4 μ L 5 M HCl. Pore water SO_4^{2-} was analyzed with ion chromatography (IC) in a
150 10-fold diluted sample (0.15 mL of pore water with 1.35 mL of de-oxygenated UHQ water). Sub-samples for DIC
151 analysis (0.5 mL) were collected in glass vials (4.9 mL) to which 4.4 mL of 25 g/L NaCl solution was added, making
152 sure that no headspace remained. Aliquots of the remaining pore water were used for the measurement of alkalinity
153 (determined onboard by titrating 1 mL of untreated sub-sample with 0.01 M HCl; results presented in the
154 Supplementary Information only) and NH_4^+ . All sub-samples were stored at 4 °C and brought to room temperature
155 just before analysis. Subsampling for sulfide was performed immediately after filtration and all other subsampling
156 was performed within 4 hours of core recovery.

157 Pore water sub-samples for HPO_4^{2-} , DIC and sulfide were directly analyzed colorimetrically onboard on two separate
158 QuAatro (SEAL Analytical, Germany) auto analyzers. HPO_4^{2-} was measured at 880 nm after the formation of
159 molybdophosphate-complexes (Murphy and Riley, 1962). Samples for DIC were acidified online after being
160 oxidized by H_2O_2 and analyzed as described by Stoll et al. (2001). To keep the dissolved sulfide in the non-volatile
161 HS^- form under alkaline conditions, 1.5 mL of 8 mM NaOH was added to the sulfide samples, which were
162 subsequently analyzed using the methylene blue method as described by Grasshoff (1969). Sub-samples for
163 dissolved Fe and Mn were analyzed onshore by ICP-OES (Perkin Elmer Optima 3000 Inductively Coupled Plasma -
164 Optimal Emission Spectroscopy). For the analysis of pore water CH_4 , a volume of 10 mL N_2 was injected into the
165 CH_4 serum flasks (while a needle inserted through the septum allowed 10 mL of water to escape) to create a
166 headspace from which a subsample was collected with a gas-tight syringe. Subsequently, CH_4 concentrations were
167 determined in the home laboratory after injection into a Thermo Finnigan Trace GC gas chromatograph (Flame
168 Ionization Detector). $\delta^{13}\text{C-CH}_4$ and $\delta\text{D-CH}_4$ (D, deuterium) were analyzed by Continuous Flow Isotope Ratio Mass
169 Spectrometry (CF-IRMS) as described in detail in (Brass and Röckmann, 2010) and (Sapart et al., 2011).

170 2.3 Bulk sediment analysis

171 Sediment samples were freeze-dried, powdered and ground in an agate mortar in an argon (Ar)-filled glove box and
172 split into oxic and anoxic fractions. Samples from the oxic fraction were used for total elemental and organic carbon
173 (C_{org}) analyses under normal atmospheric conditions, whereas anoxic splits for sediment P and Fe speciation were
174 kept under an inert, oxygen-free Ar or N_2 atmosphere at all times to avoid oxidation artefacts (Kraal and Slomp,
175 2014; Kraal et al., 2009).

176 **2.3.1 Total elemental composition and organic carbon**

177 A split of ~ 125 mg of freeze-dried sediment was dissolved overnight in 2.5 mL HF (40 %) and 2.5 mL of
178 HClO₄/HNO₃ mixture, in a closed Teflon bomb at 90 °C. The acids were then evaporated at 160 °C and the resulting
179 gel was dissolved overnight in 1 M HNO₃ at 90 °C. Total elemental concentrations in the 1 M HNO₃ solutions were
180 determined by ICP-OES. A second split of 0.3 g freeze-dried sediment was used to determine the C_{org} content using
181 an elemental analyzer (Fison Instruments model NA 1500 NCS) after carbonate removal from the sediment with two
182 washes with 1 M HCl (4 h and 12 h) followed by two washes with UHQ water and subsequent drying of the samples
183 (Van Santvoort et al., 2002).

184 **2.3.2 Sediment P fractionation**

185 To determine the solid phase partitioning of P, aliquots of 0.1 g dried sediment were subjected to the SEDEX
186 sequential extraction procedure after Ruttenberg (1992), as modified by Slomp et al. (1996b), but including the first
187 MgCl₂ step (Table 1). Sediment P was fractionated as follows: i) exchangeable-P (“P_{exch}”, extracted by 1 M MgCl₂,
188 pH 8, 0.5 h), ii) Fe-associated P (“P_{Fe}”, extracted by citrate-bicarbonate-dithionite (CDB), buffered to pH 7.5 with Na
189 citrate/Na bicarbonate, 8 h, followed by 1 M MgCl₂, pH 8, 0.5 h), iii) authigenic Ca-P (“P_{authi Ca-P}”, including
190 carbonate fluorapatite, biogenic hydroxyapatite and CaCO₃-bound P, extracted by 1 M Na acetate solution, buffered
191 to pH 4 with acetic acid, 6 h, followed by 1 M MgCl₂, pH 8, 0.5 h), iv) detrital Ca-P (“P_{detr}”, extracted by 1 M HCl,
192 24 h) and v) organic P (“P_{org}”, after ashing at 550 °C for 2 h, extracted by 1 M HCl, 24 h). The MgCl₂ washes in
193 steps ii and iii were to ensure that any HPO₄²⁻ re-adsorbed during CDB or acetate extraction was removed and
194 included in the pools of Fe-associated P and authigenic Ca-P, respectively. Sediments were shielded from oxygen
195 inside an Ar-filled glovebox until step 3 of the SEDEX procedure to eliminate the potential conversion of Ca-P to
196 Fe-bound P due to pyrite oxidation upon oxygen exposure (Kraal and Slomp, 2014; Kraal et al., 2009). Dissolved
197 HPO₄²⁻ in the CDB solution was analyzed by ICP-OES. For all other solutions, HPO₄²⁻ was determined
198 colorimetrically (Strickland and Parsons, 1972) on a Shimadzu spectrophotometer using the ammonium
199 heptamolybdate – ascorbic acid method.

200 **2.3.3 Sediment Fe fractionation**

201 Sediment Fe was fractionated into i) carbonate associated Fe (“Fe_{carb}”, including siderite and ankerite, extracted by 1
202 M Na-acetate brought to pH 4.5 with acetic acid, 24 h), ii) easily reducible (amorphous) oxides (“Fe_{ox1}”, including
203 ferrihydrite and lepidocrocite, extracted by 1 M hydroxylamine-HCl, 24 h), iii) reducible (crystalline) oxides
204 (“Fe_{ox2}”, including goethite, hematite and akagenéite, extracted by Na-dithionite buffer, pH 4.8, 2 h) and iv) Fe in
205 recalcitrant oxides (mostly magnetite, “Fe_{mag}”, extracted by 0.2 M ammonium oxalate / 0.17 M oxalic acid solution,
206 2 h), according to Poulton and Canfield (2005), using a 50 mg aliquot of dried sediment (Table 1). An additional
207 aliquot of 50 mg was subjected to an adapted sequential extraction procedure after Claff et al. (2010), separating
208 labile Fe(II) (“Fe(II)_{HCl}”) and Fe(III) (“Fe(III)_{HCl}”) using 1 M HCl (4 h) from crystalline Fe oxide minerals
209 (“Fe(II)_{CDB}”, Na-dithionite buffer, pH 4.8, 4 h) and from pyrite (“Fe_{pyrite}”, concentrated nitric acid, 2 h), for all
210 multicores as well as for the long core at site 4 (Table 1).

211 At site 4 (multicore only) and 5 (multicore and gravity core), aliquots of 0.5 g dried sediment were used to
 212 sequentially determine the amount of FeS (acid volatile sulfur, “AVS”, using 6 M HCl) and FeS₂ (chromium
 213 reducible sulfur, “CRS”, using acidic chromous chloride solution) via the passive diffusion method described by
 214 (Burton et al., 2008) using iodometric titration of the ZnS formed in the alkaline Zn acetate traps to quantify AVS
 215 and CRS (Table 1).

216 2.4 Diagenetic model

217 2.4.1 General form

218 A multicomponent transient diagenetic model was developed for site 4 based on existing diagenetic models (Reed et
 219 al., 2011a, 2011b; Rooze et al., 2016) to gain a better understanding of the transient diagenesis in Black Sea
 220 sediments and to investigate the potential for Fe-AOM as a source of pore water Fe²⁺ at depth. The model describes
 221 the cycling of dissolved and particulate chemical species in a 1D sediment column (Berner, 1980). A total of 25
 222 different chemical species (Table 2) were subjected to a suite of biogeochemical reactions (Table 3) and vertical
 223 transport through burial, as well as molecular diffusion for dissolved species (Boudreau, 1997; Soetaert et al., 1996;
 224 Wang and Van Cappellen, 1996). The general diagenetic equations for solid (Eq. (1)) and dissolved species (Eq. (2))
 225 are, respectively,

$$226 (1 - \phi) \frac{\partial C_S}{\partial t} = -(1 - \phi)v \frac{\partial C_S}{\partial x} + \sum R_S \quad (1)$$

$$227 \phi \frac{\partial C_{aq}}{\partial t} = \phi D' \frac{\partial^2 C_{aq}}{\partial x^2} - \phi u \frac{\partial C_{aq}}{\partial x} + \sum R_{aq} \quad (2)$$

228 where C_S is the concentration of the solid species (mol L⁻¹; mass per unit volume of solids), C_{aq} the concentration of
 229 the dissolved species (mol L⁻¹; mass per unit volume of pore water), t is time (yr), ϕ the sediment porosity, x the
 230 distance from the sediment-water interface (cm), D' the diffusion coefficients of dissolved species in the sediment
 231 (cm² yr⁻¹) adjusted for the considered setting (Supplementary Table S1) (Boudreau, 1997) and corrected for the
 232 tortuosity in the porous medium (Boudreau, 1996) (see Supplementary Information). $\sum R_S$ and $\sum R_{aq}$ are the net
 233 reaction rates of the solid and dissolved species from the chemical reactions they participate in (Table 3), and v and
 234 u the advective velocities (cm yr⁻¹) of the solid and the dissolved species, respectively. Porosity and advective
 235 velocities were described by depth-dependent functions to account for sediment compaction (Meysman et al., 2005;
 236 Reed et al., 2011a) (see Supplementary Information and Supplementary Fig. S1).

237 Reactions considered by the model and corresponding reaction equations are given in Tables 3 and 4, respectively,
 238 and are divided into primary redox reactions and other biogeochemical reactions, including various mineral
 239 formation and dissolution reactions (Reed et al., 2011a, 2011b; Rooze et al., 2016). Corresponding reaction
 240 parameters were mostly taken from the literature or, if these were not available or no fit to the data could be obtained
 241 with existing parameter ranges, constrained using the extensive geochemical dataset for site 4 (Table 5). **A model
 242 sensitivity analysis for key parameters is provided in the Supplementary Information (Supplementary Figs. S2 and
 243 S3).**

244 To account for differences in reactivity and crystallinity between different species, organic matter and Fe oxides are
 245 divided into three different pools, representing highly reactive (α), less reactive (β) and non-reactive (i.e. inert) (γ)

246 phases. For the Fe oxides, only the α phase is used by organoclastic Fe reduction (Table 3), while the β phase is also
247 used by Fe-AOM. This assumption was made to test whether the pore water and sediment profiles observed in the
248 Black Sea can be reproduced with Fe-AOM as the main Fe reduction pathway at depth. In addition, it allows an
249 assessment of the potential impact of Fe-AOM on sedimentary CH_4 cycling. Note that, as a consequence of the
250 exclusion of organoclastic Fe reduction at depth, the model results should not be interpreted as proof for Fe-AOM
251 but rather imply that it is a possible mechanism.

252 The succession of oxidants during organic matter decomposition (Froelich et al., 1979) is described by means of
253 Monod kinetics (Table 4), whereby those oxidants with the highest metabolic free energy yield are used
254 preferentially until they become limiting and the oxidant with the next highest energy yield is used (Berg et al., 2003;
255 Boudreau, 1996; Reed et al., 2011b; Rooze et al., 2016; Wang and Van Cappellen, 1996). Oxidants considered by the
256 model are (in descending order of energy yield) O_2 , nitrate (NO_3^-), Fe oxides and SO_4^{2-} . Once these oxidants are
257 exhausted, organic matter remineralization occurs by methanogenesis. Corresponding limiting concentrations for the
258 oxidants are taken from (Reed et al., 2011a) (Table 5). In addition, an attenuation factor, Ψ , is used to slow down
259 anaerobic organic matter degradation through SO_4^{2-} reduction and methanogenesis, thus allowing for better
260 preservation of organic matter under anoxic bottom water conditions (Moodley et al., 2005; Reed et al., 2011a,
261 2011b).

262 Cycling of S is simulated using five different chemical species, i.e. Fe monosulfides (FeS), pyrite (FeS_2), elemental S
263 (S_0), dissolved sulfide and pore water SO_4^{2-} (Table 2), combined in a network of various biogeochemical reactions
264 (Table 3). The CH_4 cycle includes CH_4 production from organic matter and from DIC (i.e. CO_2), as well as CH_4
265 oxidation coupled to the reduction of O_2 , SO_4^{2-} and $\text{Fe}(\text{OH})_3$ (Table 3). For AOM a bimolecular rate equation was
266 used (Table 4), which is the most common way to parameterize AOM in reactive transport models (Regnier et al.,
267 2011) and allows the use of largely unknown half-saturation constants, in particular for the putative Fe-AOM
268 pathway, to be avoided. Although Mn-oxides have also been suggested to be a thermodynamically favorable electron
269 acceptor for AOM (Beal et al., 2009), they were not included in the model because of the relatively low Mn
270 concentrations ($\sim 15 \mu\text{mol g}^{-1}$ for total sedimentary Mn and $< 30 \mu\text{M}$ for dissolved Mn^{2+} ; Supplementary Fig. S2 and
271 S3) when compared to Fe and the likely presence of most of the Mn in the form of Mn-carbonates.

272 The P forms included in the model are pore water HPO_4^{2-} , authigenic Ca-P, organic P and detrital P, as well as Fe-
273 bound P, i.e. P associated with Fe oxides and P in vivianite (Table 2). The removal of dissolved Fe^{2+} through
274 formation of the Fe minerals FeS, siderite (FeCO_3) and vivianite is also included in the model (Table 3). Mass
275 balances for all chemical species included in the model are given in Supplementary Table S2.

276 The boundary conditions at the sediment surface were specified as time-dependent depositional fluxes for the
277 particulate components and as fixed bottom water concentrations for the dissolved species, while a zero gradient
278 boundary condition was set for all chemical species at the base of the model domain (Fig. 2 and Supplementary
279 Table S3). To avoid potential interferences of the lower boundary conditions with the model results in the upper
280 sediments (see Supplementary Fig. S6), the model depth was set to 3000 cm and divided into 500 grid cells. The
281 thickness of the upper layer was set at 1 cm, and the thickness of the following grid layers increased exponentially to
282 ~ 6 cm at 800 cm depth and to ~ 18 cm at 3000 cm depth. In this paper, only the upper 800 cm are shown. However,
283 all profiles extending over the full depth range are provided in the Supplementary Information file (Supplementary

284 Fig. S5 and Fig. S7). The model code was written in R using the marelac geochemical dataset package (Soetaert et
285 al., 2010) and the ReacTran package (Soetaert and Meysman, 2012) to calculate the transport in porous media. The
286 set of ordinary differential equations was subsequently solved numerically with the lsoda integrator algorithm
287 (Hindmarsh, 1983; Petzoldt, 1983)

288 2.4.2 Transient scenario

289 The model applied in this study simulates the sediment deposition during the last 25000 years. A constant mass
290 accumulation rate of $0.06 \text{ g cm}^{-2} \text{ yr}^{-1}$ over the Holocene was assumed. In order to reduce the computing time for the
291 freshwater period, a higher mass accumulation rate of $1 \text{ g cm}^{-2} \text{ yr}^{-1}$ was used between 25000 and 10000 years before
292 present (B.P.) and all fluxes were corrected accordingly (i.e. multiplied with a factor of 16.67). Inflow of
293 Mediterranean saltwater into the Black Sea basin was modelled assuming an initial salinity of 1 for the freshwater
294 lake and a linear increase to a salinity of 22 between 8500 and 1500 years B.P. (Fig. 2). Such a salinization scenario
295 results in a good fit to the chloride (Cl^-) profile (Fig. 3) and compares well with a previous salinity reconstruction
296 suggesting a linear increase in salinity of 1 to 22 between 9000 ± 500 years B.P. and 2000 ± 500 years B.P. (Soulet et
297 al., 2010). Bottom water salinity was converted to Cl^- and SO_4^{2-} using the molecular weights and seawater density
298 derived from the marelac geochemical dataset package (Soetaert et al., 2010) (Supplementary Table S1). A shift
299 from oxic towards euxinic conditions around 7600 years B.P., with a peak in organic matter loading around 5300
300 years B.P. and constant elevated organic matter fluxes after 2700 years B.P. was assumed, following a recent study
301 comprising data from seven sediment cores collected from the Black Sea (Eckert et al., 2013) (Fig. 2). In addition,
302 the input of organic matter was assumed to increase again in the last century, reflecting anthropogenic eutrophication
303 of waters on the adjacent continental shelf as previously reported (Capet et al., 2013; Kemp et al., 2009). With the
304 development of anoxic and sulfidic bottom-water conditions, depositional fluxes of reactive Fe oxides were assumed
305 to be zero (Fig. 2). In contrast, fluxes of Fe sulfides are high under euxinic conditions and dominated by FeS_2 .

306 3 Results

307 3.1 Pore water profiles

308 Pore water profiles of SO_4^{2-} show a linear decrease from $\sim 17 \text{ mM}$ at the sediment water interface to a depth of ~ 230
309 cm at both sites, below which CH_4 starts to accumulate in the pore water (Fig. 3). Bubble formation and degassing of
310 CH_4 during gravity coring could not be avoided because of the high concentrations of CH_4 in the limnic deposits
311 above the saturation of ca 1.3 mM CH_4 at atmospheric pressure (calculated for a salinity of 22 and a temperature of
312 $25 \text{ }^\circ\text{C}$ using the algorithm from Mogollón et al. (2013)). Observations of increased outgassing with depth during
313 coring suggest that the low CH_4 concentrations in the deeper sediments at both sites are due to enhanced outgassing
314 with increasing levels of CH_4 . Pore water profiles of NH_4^+ at both sites are similar and concentrations increase to ~ 3
315 mM at depth, suggesting that actual CH_4 concentrations at both sites could be comparable. Most of the CH_4 values
316 thus only indicate the presence or absence of CH_4 and are not a quantitative measure (indicated as open diamonds in
317 Fig. 4). Note that the upper $\sim 300 \text{ cm}$ of sediment at site 5 are likely less affected by CH_4 outgassing. Modeled pore

318 water concentrations of CH₄ on the other hand, show a steep increase below the SMTZ, comparable to the gradient
319 observed at site 5, and build up to concentrations of ~ 15 mM at depth (Supplementary Fig. S5).

320 The SMTZ is located around 230 cm depth in the sediment and is characterized by the removal of both pore water
321 SO₄²⁻ and dissolved CH₄. In this zone, SO₄-AOM drives the production of dissolved sulfide, DIC and alkalinity
322 (Supplementary Fig. S5) and diffusion of these pore water constituents away from the SMTZ (Fig. 3). Below the
323 sulfide diffusion front, Fe²⁺ accumulates in the pore water. Dissolved HPO₄²⁻ reaches a maximum around the depth
324 where sulfide levels drop below the detection limit of 1 μmol L⁻¹, followed by a steep decrease with depth.
325 Concentrations of pore water Mn²⁺ are more than an order of magnitude lower than those of dissolved Fe²⁺, and
326 decrease from the sediment surface until ~ 200 cm depth, below which they slightly increase again (Supplementary
327 Fig. S5).

328 The smooth pore water profiles of δ¹³C-CH₄ and δD-CH₄ suggest that the isotopic composition of pore water CH₄
329 (available for site 5 only) is less affected by the CH₄ loss and reveals a biological origin in the limnic deposits, with
330 hydrogenotrophic carbonate reduction, i.e. microbial reduction of CO₂ to CH₄ as the main methanogenic pathway for
331 the range of CH₄ isotope ratios observed in these sediments (Fig. 4) (Whiticar, 1999). Upward diffusing CH₄ shows a
332 gradual depletion in δ¹³C-CH₄ from ~ -74 ‰ at depth to ~ -96 ‰ around the SMTZ, followed by subsequent
333 progressive ¹³C enrichment towards the sediment surface. δD-CH₄ shows a small enrichment from -226 ‰ at depth
334 to ~ -208 ‰ at the SMTZ and a strong shift towards high δD-CH₄ values of up to ~ 113 ‰.

335 3.2 Solid phase profiles

336 A pronounced excursion in sedimentary C_{org} at site 4 in combination with a shift from gray clay deposits to micro-
337 laminated black sediments indicates that the lake-marine transition, i.e. the transition between the marine sapropel
338 Unit II and the deep limnic sediments of Unit III (Arthur and Dean, 1998; Degens and Ross, 1974), is located around
339 a sediment depth of ~ 90 cm at site 4 (Fig. 5). At site 5, Unit I and Unit II were lost due to a turbidite, explaining the
340 low concentrations of C_{org} in the upper sediments.

341 Concentrations of solid S increase with decreasing depth from 20 μmol g⁻¹ below 300 cm (sulfidization front) to ~
342 400 μmol g⁻¹ in the upper 100 cm at both sites and are dominated by FeS₂ (Fig. 5). Iron oxides show a decrease from
343 ~ 100 μmol g⁻¹ at depth to ~ 50 μmol g⁻¹ in the sediments between 100 – 300 cm and a further decrease to ~ 10 μmol
344 g⁻¹ closer to the sediment surface. Amorphous Fe oxides (Fe_{ox1}) and more crystalline oxides (Fe_{ox2}) both account for
345 half the total amount of Fe oxides, with a small contribution of recalcitrant oxides (Fe_{mag}) (Supplementary Fig. S4).
346 The results from the two different Fe extractions applied in this study (Table 1) generally compare well
347 (Supplementary Fig. S4). Note, however, that the Fe oxides in Fig. 5 represent the results from the extraction after
348 Poulton and Canfield (2005). Results from the Fe extractions modified from Claff et al. (2010) are provided in the
349 Supplementary Information only. Sedimentary Mn content is relatively low at all three sites, ranging from ~ 5-10
350 μmol g⁻¹ in the marine sediments to ~ 15 μmol g⁻¹ in the deep limnic deposits of Unit III (Supplementary Fig. S4).
351 Sediments below the sulfidization front are characterized by high Fe carbonate contents of ~ 100 μmol g⁻¹. The sharp
352 depletion in Fe carbonate around the sulfidization front could only be reproduced in the model by assuming Fe

353 carbonate dissolution by dissolved sulfide (Table 3). These results suggest a conversion of reactive Fe from
354 carbonate toward sulfide phases in the presence of abundant dissolved sulfide.

355 Units I and II show high concentrations of organic P, which accounts for ~ 30 % of total P in these sediments (Fig.
356 5). Low organic P and high concentrations of detrital P in the upper sediments at site 5 are due to the turbidite. The
357 limnic deposits of Unit III are generally depleted in organic P (< 6 % of total P) and enriched in detrital P.
358 Authigenic Ca-P shows little variation in the sediments of Unit III, accounting for ~ 20 to 30 % of total P at the two
359 sites. The contribution of Fe-associated P, on the other hand, is reduced in the limnic deposits of Unit III exposed to
360 the downward diffusing sulfide (~ 20 %) when compared to the sediments below the sulfidization front (~ 30 %).
361 Concentrations of exchangeable P are < 2 $\mu\text{mol g}^{-1}$ for sediments above the SMTZ and < 1 $\mu\text{mol g}^{-1}$ for sediments at
362 depth (data not shown).

363 Modeled SO_4^{2-} reduction rates show two distinct peaks of ~ 200 $\text{pmol SO}_4^{2-} \text{cm}^{-3} \text{d}^{-1}$ in the sediments of Unit II and
364 in the sediments around the SMTZ (Fig. 6). Rates of CH_4 production are highest (~ 30 $\text{pmol CH}_4 \text{cm}^{-3} \text{d}^{-1}$) in the
365 organic-rich marine deposits of Unit II and in the limnic deposits below the SMTZ. The sediments around the SMTZ
366 are further characterized by high rates of SO_4 -AOM (~ 200 $\text{pmol cm}^{-3} \text{d}^{-1}$), whereas sediments directly below the
367 sulfidization front show enhanced rates of S_0 disproportionation (~ 15 $\text{pmol cm}^{-3} \text{d}^{-1}$). Organoclastic SO_4^{2-} reduction
368 provides the main source for pore water sulfide in the organic-rich marine deposits, while SO_4 -AOM and S_0
369 disproportionation are the dominant sources of dissolved sulfide in sediments around the SMTZ and directly below
370 the sulfidization front, respectively. Rates of Fe-AOM are generally low (< 0.04 $\text{pmol CH}_4 \text{cm}^{-3} \text{d}^{-1}$) and restricted to
371 the limnic deposits only.

372 **3.3 Temporal evolution**

373 The temporal evolution in pore water and solid phase constituents illustrates the impact of the lake-marine transition
374 on the sediment geochemistry (Fig. 7). Concentrations of pore water Cl^- and SO_4^{2-} increase with the intrusion of
375 marine Mediterranean Sea waters, accompanied by a decrease in dissolved CH_4 and accumulation of pore water
376 sulfide in the shallower sediments. Dissolved Fe^{2+} becomes restricted to non-sulfidic pore waters at depth, while
377 HPO_4^{2-} and solid S start to accumulate in the presence of dissolved sulfide. Iron oxides decrease in the surface
378 sediments as well as in the sediments at depth. Vivianite, on the other hand, becomes increasingly enriched in
379 sediments below the downward diffusing sulfide front.

380 **4. Discussion**

381 **4.1 Coupled S, CH_4 and Fe dynamics**

382 **4.1.1 Organoclastic SO_4^{2-} reduction**

383 Model-derived areal rates of total SO_4^{2-} reduction of ~ 0.24 $\text{mmol SO}_4^{2-} \text{m}^{-2} \text{d}^{-1}$ (Table 6), i.e. the total amount of
384 SO_4^{2-} reduced per square meter of sea floor, compare well with calculated diffusive fluxes of SO_4^{2-} into the sediment
385 at sites 4 and 5 (~ 0.21 and 0.20 $\text{mmol SO}_4^{2-} \text{m}^{-2} \text{d}^{-1}$, respectively) and are in good agreement with previous SO_4^{2-} flux
386 estimates of 0.17 to 0.28 $\text{mmol SO}_4^{2-} \text{m}^{-2} \text{d}^{-1}$ for sediments of the western Black Sea (Jørgensen et al., 2001). In the

387 model, organoclastic SO_4^{2-} reduction accounts for > 65 % of total organic matter degradation in the upper 800 cm of
388 sediment, supporting previous conclusions that SO_4^{2-} reduction represents the dominant mineralization process of
389 organic matter in sediments below the chemocline (Jørgensen et al., 2001; Thamdrup et al., 2000). The remaining <
390 25 % of organic matter remineralization is due to methanogenesis. The relative contribution of SRR to organic
391 matter remineralization, however, likely is significantly higher when taking into account the high SRR in the
392 uppermost sediment layers (Jørgensen et al., 2001), which are not captured by our model.

393 The depth-dependent rate profile of SO_4^{2-} reduction shows two distinct peaks of ~ 70 and $230 \text{ pmol SO}_4^{2-} \text{ cm}^{-3} \text{ d}^{-1}$
394 associated with organoclastic SO_4^{2-} reduction in the organic matter rich marine deposits of Unit I and Unit II. These
395 rates are at the low end of reported values from Black Sea sediments ($0.1 - 20 \text{ nmol cm}^{-3} \text{ d}^{-1}$) (Holmkvist et al.,
396 2011b; Jørgensen et al., 2001, 2004; Knab et al., 2009; Leloup et al., 2007). Our model further demonstrates that the
397 two SRR peaks in the sediments of Unit I and Unit II are not reflected in the pore water profile of SO_4^{2-} . This finding
398 is in line with earlier work showing that the SO_4^{2-} gradient in Black Sea sediments is primarily affected by SO_4 -
399 AOM in the SMTZ (Jørgensen et al., 2001). The shorter diffusion distance (the diffusion time to ~ 200 cm is about 5
400 times longer than to ~ 90 cm, i.e. ~ 300 years vs. ~ 60 years) and higher porosity in Unit I and II (Supplementary Fig.
401 S1) both dampen the effect of SO_4^{2-} reduction in the marine deposits on the SO_4^{2-} profile (see also Jørgensen et al.,
402 2001). Thus, our results support previous conclusions that SRR estimates based on pore water profiles of SO_4^{2-} (i.e.
403 net SO_4^{2-} consumption) alone may underestimate the actual SO_4^{2-} turnover (i.e. gross SO_4^{2-} reduction) in marine
404 sediments (Jørgensen, 1978; Jørgensen et al., 2001).

405 4.1.2 SO_4 -AOM

406 Pore water profiles of SO_4^{2-} , CH_4 , sulfide and DIC reveal a distinct SMTZ around 230 cm depth at both sites, where
407 SO_4 -AOM with upward diffusing CH_4 results in the concomitant removal of pore water SO_4^{2-} and CH_4 and in the
408 accumulation of dissolved sulfide and DIC in the pore waters of these sediments (Fig. 3). The depth of the SMTZ
409 and the steep increase in CH_4 to > 3 mM below the SMTZ found in this study are consistent with earlier observations
410 in sediments of the western Black Sea (Henkel et al., 2012; Holmkvist et al., 2011b; Jørgensen et al., 2001, 2004;
411 Knab et al., 2009; Leloup et al., 2007). The location of the SMTZ, however, has progressed downwards in the last ca.
412 9000 years, following the inflow of SO_4^{2-} -rich salt water into the Black Sea basin (Fig. 7) (see also Henkel et al.,
413 2012)).

414 Calculated diffusive fluxes of SO_4^{2-} and CH_4 to the SMTZ ($\sim 0.2 \text{ mmol SO}_4^{2-} \text{ m}^{-2} \text{ d}^{-1}$ and $0.08 \text{ mmol CH}_4 \text{ m}^{-2} \text{ d}^{-1}$) and
415 modelled areal rates of SO_4 -AOM ($\sim 0.16 \text{ mmol m}^{-2} \text{ d}^{-1}$) suggest that AOM accounts for ~ 40 to 70 % of the total
416 SO_4^{2-} reduction in these sediments, with the remaining ~ 30 to 60 % attributed to organoclastic SO_4^{2-} reduction. Such
417 a high contribution of AOM exceeds the range of previous estimates that included experimentally measured SRR
418 close to the sediment surface (~ 7 to 18 %) (Jørgensen et al., 2001, 2004). Around the SMTZ, SO_4 -AOM is
419 responsible for ~ 97 % of the total SO_4^{2-} reduction (Fig. 6 and Table 6), thus enhancing the downward diffusive flux
420 of sulfide into the deep limnic deposits of Unit III. Our model suggests that without this additional source of sulfide
421 through SO_4 -AOM, the sulfidization front would currently be located around 150 cm depth in the sediment (Fig. 8).

422 The consumption of upward diffusing CH₄ by SO₄²⁻-driven AOM leads to a progressive enrichment of ¹³C and D in
423 the residual CH₄ above the SMTZ (Fig. 4) due to the preferential oxidation of isotopically light CH₄ during SO₄-
424 AOM (Alperin et al., 1988; Martens et al., 1999; Whiticar, 1999). Interestingly, pore water CH₄ above the SMTZ
425 shows unusually high δD-CH₄ values that fall outside of the common range observed for pore water δD-CH₄ (e.g.
426 Whiticar et al., 1999). Future studies, however, are needed to resolve the cause of the strong D-enrichment of
427 dissolved CH₄ above the SMTZ in Black Sea sediments.

428 Modeled concentrations of CH₄ indicate that the measurements above the sulfidization front at site 5 are likely less
429 affected by outgassing during core recovery (Fig. 4) and can thus be used to derive kinetic isotope fractionation
430 factors for carbon (ε_C) and hydrogen (ε_H) associated with SO₄-AOM at the SMTZ using the Rayleigh distillation
431 function (Crowe et al., 2011; Egger et al., 2015b; Rayleigh, 1896; Whiticar, 1999). Note that the Rayleigh distillation
432 function only applies to closed systems (Rayleigh, 1896). However, considering that diffusion could be slower than
433 oxidation in deep sediments of the Black Sea, these sediments may represent a quasi-closed system. Corresponding
434 estimates for ε_C of ~ 8 ‰ (R² = 0.972) and ε_H of ~ 58 ‰ (R² = 0.982) are at the lower end of previously documented
435 values in marine and brackish-marine environments (8-38 ‰ for ε_C and 100-324 ‰ for ε_H) (Alperin et al., 1988;
436 Egger et al., 2015b; Holler et al., 2009; Martens et al., 1999; Reeburgh, 2007). These values should be interpreted as
437 an approximation, as more accurate estimates would require isotope modeling (e.g. Alperin et al., 1988).

438 At the base of the SMTZ, upward diffusing CH₄ reveals an initial depletion in δ¹³C-CH₄ (Fig. 4). Such a shift to ¹³C-
439 depleted CH₄ together with a decrease in its concentration could indicate an enzyme-mediated equilibrium C isotope
440 exchange during SO₄-AOM at low SO₄²⁻ concentrations (< 0.5 mM) (Holler et al., 2012; Yoshinaga et al., 2014). The
441 effect of such mechanisms on deuterated CH₄ is likely limited.

442 4.1.3 Cryptic S cycling

443 Earlier studies showed evidence for ongoing SO₄²⁻ reduction (< 1 nmol cm⁻³ d⁻¹) within the SO₄²⁻-depleted (< 0.5
444 mM) limnic deposits below the SMTZ in sediments of the Black Sea (Holmkvist et al., 2011b; Knab et al., 2009;
445 Leloup et al., 2007), Baltic Sea (Holmkvist et al., 2011a, 2014; Leloup et al., 2009) and Alaskan Beaufort Sea
446 (Treude et al., 2014) likely driven by SO₄²⁻ production from re-oxidation of dissolved sulfide with oxidized Fe
447 minerals. In this mechanism, Fe oxides enhance the recycling of sulfide to SO₄²⁻ in a cryptic S cycle (Holmkvist et
448 al., 2011a; Treude et al., 2014) thereby fueling SO₄²⁻-driven AOM in Fe oxide-rich sediments. In this cryptic S cycle,
449 dissolved sulfide is oxidized to zero-valent sulfur (S₀), a key intermediate in AOM, which is subsequently
450 disproportionated to SO₄²⁻ and sulfide by associated Deltaproteobacteria (Holmkvist et al., 2011a; Milucka et al.,
451 2012; Sivan et al., 2014; Treude et al., 2014). The additional SO₄²⁻, produced during S₀ disproportionation, may then
452 be re-used by the methanotrophic archaea as an electron acceptor for SO₄-AOM (Milucka et al., 2012).

453 Our model results suggest slow rates of ongoing SO₄²⁻ reduction of < 0.2 nmol cm⁻³ d⁻¹ (Fig. 6) within the limnic
454 deposits below the SMTZ exposed to dissolved sulfide (Table 6), in line with estimated SRR based on ³⁵SO₄²⁻
455 incubation experiments with Black Sea sediments from below the SMTZ of ~ 0.1-0.5 nmol cm⁻³ d⁻¹ (Knab et al.,
456 2009; Leloup et al., 2007). Below the sulfidization front, SRR show a distinct peak of ~ 5 pmol cm⁻³ d⁻¹. Active SO₄²⁻
457 reduction in these SO₄²⁻-depleted sediments requires deep SO₄²⁻ formation to maintain low net rates of SO₄²⁻

458 reduction. In the model, S_0 disproportionation is the only potential source of pore water SO_4^{2-} at depth (Table 3).
459 Formation of S_0 , in turn, occurs exclusively by oxidation of dissolved sulfide during the reductive dissolution of Fe
460 oxides, explaining the distinct S_0 disproportionation peak of $\sim 15 \text{ pmol cm}^{-3} \text{ d}^{-1}$ around the sulfidization front (Fig. 6).
461 Thus, based on the model assumptions, we conclude that Fe oxides increase the transformation of sulfide to SO_4^{2-} via
462 formation and subsequent disproportionation of S_0 in these sediments, as suggested previously (Holmkvist et al.,
463 2011b; Knab et al., 2009; Leloup et al., 2007). Such recycling of SO_4^{2-} stimulates slow rates of SO_4 -AOM in the
464 sediments below the SMTZ, explaining the low background rates of SO_4^{2-} reduction in the SO_4^{2-} -depleted limnic
465 deposits. These results support recent findings of indirect Fe stimulated SO_4^{2-} driven AOM in laboratory experiments
466 (Sivan et al., 2014), and highlight that Fe oxides could play a significant role as stimulators of AOM and S recycling
467 in natural environments.

468 **4.2 Fe reduction below the sulfidization front**

469 Below the sulfidization front, Fe^{2+} starts to accumulate in the pore water (Fig. 3). Although previous studies have
470 also reported an increase of dissolved Fe^{2+} around the depth where sulfide levels drop below the detection limit
471 (Holmkvist et al., 2011b; Jørgensen et al., 2004; Knab et al., 2009), the source of this pore water Fe^{2+} has remained
472 unknown. One possible explanation could be that the elevated Fe^{2+} concentrations at depth represent remnant Fe^{2+}
473 accumulated during the Black Sea “Lake” phase (Knab et al., 2009). In our model, Fe^{2+} shows a broad peak of ~ 300
474 μM until ~ 300 cm depth in the sediment during the initial Lake phase, assuming organoclastic Fe reduction as the
475 only Fe reduction pathway (data not shown). The removal of Fe^{2+} through authigenic formation of reduced Fe(II)
476 minerals, however, prevents the accumulation of substantial amounts of Fe^{2+} in the pore water below ~ 300 cm
477 sediment depth during the Lake phase (Fig. 8). We therefore conclude that the high concentrations of dissolved Fe^{2+}
478 below the sulfidization front are most likely indicative of active Fe reduction in these sediments.

479 **4.2.1 Fe reduction through cryptic S cycling**

480 In theory, a cryptic S cycle, as described in section 4.1.3, could result in net accumulation of dissolved Fe^{2+} if the
481 sulfide consumption from reaction with ferric Fe outweighs the production of sulfide from SO_4^{2-} reduction. Modeled
482 Fe^{2+} indeed shows a peak of $< 100 \mu\text{M}$ directly below the sulfidization front, assuming no active Fe reduction in the
483 limnic deposits (Fig. 8). Model simulations further indicate that, based on the reaction network used in this study
484 (Table 3), cryptic S cycling could result in a build up of pore water Fe^{2+} of $\sim 300 \mu\text{M}$ at depth in the sediment
485 provided there was no precipitation of reduced Fe(II) minerals (Supplementary Fig S2). However, concentrations of
486 dissolved Fe^{2+} are too low compared to the measurements and confined to sediments between 300 – 400 cm depths
487 only. The diagenetic model developed in this study therefore suggests that cryptic S cycling is unlikely to explain the
488 high concentrations ($\sim 800 \mu\text{M}$) of dissolved Fe^{2+} observed in the deep limnic deposits.

489 **4.2.2 Organoclastic Fe reduction**

490 In the model, the reduction of Fe oxides coupled to organic matter degradation only occurs with the easily reducible
491 α phase in order to allow for the burial of the more crystalline β phase at depth (Table 3). Since the α phase is

492 efficiently reduced in the upper few centimeters during organoclastic Fe reduction, no easily reducible Fe oxides are
493 being buried into the deep sediments in the diagenetic model. Organoclastic Fe reduction therefore does not occur
494 within the modeled deep limnic deposits that exclusively contain more crystalline (β) and refractory (γ) Fe oxides
495 (Fig. 5). Instead, we assume that CH_4 represents a plausible electron donor for the reduction of more crystalline Fe
496 oxides in the organic-poor deep sediments with relatively refractory old organic matter (< 0.8 wt %). **The exclusion
497 of organoclastic Fe reduction at depth in the model provides an estimate of an upper constraint on the potential
498 importance of Fe-AOM in Black Sea sediments. As a result of this assumption, however, the model results cannot be
499 used to conclude whether Fe-AOM is more likely than organoclastic Fe reduction.**

500 An increasing body of geochemical evidence and laboratory incubation experiments shows that Fe-AOM might be
501 occurring in a variety of different aquatic environments (Amos et al., 2012; Beal et al., 2009; Crowe et al., 2011;
502 Egger et al., 2015b; Riedinger et al., 2014; Scheller et al., 2016; Segarra et al., 2013; Sivan et al., 2011; Wankel et
503 al., 2012). In addition, several studies have shown that Fe-reducing microorganisms are able to outcompete
504 methanogens for common substrates (e.g. acetate and H_2), thus reducing the concentrations of these common
505 primary electron donors to levels that are too low for methanogens to grow (Acht nich et al., 1995; Lovley and
506 Phillips, 1987; Lovley et al., 1989). These results, together with the observed capability of methanogens to switch
507 from CH_4 production to Fe reduction (Bodegom et al., 2004; Bond and Lovley, 2002; Liu et al., 2011; Reiche et al.,
508 2008; Sivan et al., 2016; Vargas et al., 1998) led to the common conclusion that Fe oxides exert a suppressive effect
509 on methanogenesis. Ongoing CH_4 production in the Fe oxide-rich limnic deposits, as deduced from the isotopic
510 composition of pore water CH_4 (Fig. 4) could then indicate limited organoclastic Fe reduction in these sediments.

511 However, there is increasing evidence that (semi)conductive crystalline Fe oxides (e.g. hematite and magnetite) can,
512 in fact, stimulate concurrent methanogenesis and organoclastic Fe reduction through direct interspecies electron
513 transfer (DIET), by serving as electron conduits among syntrophic CH_4 -producing organisms at rates that are
514 substantially higher than those for interspecies electron transfer by H_2 (Cruz Viggi et al., 2014; Kato et al., 2012; Li
515 et al., 2014; Zhou et al., 2014; Zhuang et al., 2015). The inhibitory effect of Fe reduction on methanogenesis thus
516 appears to be lower for crystalline Fe oxides such as hematite and magnetite, which are less bioavailable to Fe-
517 reducing organisms than poorly crystalline (amorphous) Fe oxides (e.g. ferrihydrite and lepidocrocite) (Lovley,
518 1991; Qu et al., 2004; Zhuang et al., 2015). These findings indicate that the crystallinity and conductivity of Fe
519 oxides may play a key role in determining whether methanogenesis is stimulated or suppressed in Fe oxide-rich
520 environments. In addition, the presence of methanogens that are able to rapidly switch between methanogenesis and
521 reduction of Fe oxides could also result in a reactivation of less reactive Fe oxides that were not reduced during
522 initial organoclastic Fe reduction in the deep methanogenic zone as suggested by Sivan et al. (2016). Thus, the deep
523 limnic sediments may be characterized by a complex interplay of concurrent methanogenesis, Fe oxide reduction and
524 methanotrophy, i.e. AOM.

525 **4.2.3 Fe-AOM**

526 Our model results indicate that Fe-AOM could also be a possible mechanism explaining the buildup of pore water
527 Fe^{2+} below the sulfidization front. Previous studies have shown that in systems where production and oxidation of

528 CH₄ take place concurrently, methanogenesis might conceal the isotopic signature of AOM (Egger et al., 2015b;
529 Seifert et al., 2006; Whiticar, 1999). Thus, unlike SO₄-AOM, Fe-dependent AOM likely only has little effect on the
530 isotopic composition of pore water CH₄ due to the removal of small amounts of CH₄ in sediments with ongoing
531 methanogenesis. This might explain why pore water CH₄ does not show enrichment in both heavy isotopes below the
532 sulfidization front as would be expected if Fe-AOM would occur, but rather indicates antipathetic changes, i.e.
533 depletion in ¹³C-CH₄ and enrichment in D-CH₄, usually attributed to CH₄ production from carbonate reduction
534 (Chanton et al., 2005; Whiticar, 1999).

535 Model derived rates for Fe-AOM of ~ 0.04 pmol cm⁻³ d⁻¹ (Fig. 6) are significantly lower than potential Fe-AOM
536 rates of ~ 4 nmol cm⁻³ d⁻¹ estimated from laboratory incubation studies (Egger et al., 2015b; Segarra et al., 2013;
537 Sivan et al., 2011) with brackish and limnic sediment samples. This large deviation is likely due to an overestimation
538 of Fe-AOM rates derived from stimulated microbial communities under laboratory conditions using freshly
539 synthesized and thus easily bioavailable Fe oxides when compared to in-situ conditions.

540 In the upper 800 cm of sediment, Fe-AOM accounts for < 1 % of total CH₄ oxidation, with the remaining > 99 %
541 attributed to SO₄-AOM (Table 6; see also Supplementary Fig. S2). However, while high rates of SO₄-AOM are
542 mainly restricted to the SMTZ, Fe-AOM might occur over a deep methanogenic zone, reaching far down into the
543 sediment. To accurately assess the contribution of Fe-AOM to the total CH₄ consumption in Black Sea sediments,
544 additional knowledge about the vertical expansion of the Fe oxide-rich limnic sediments deposited during the Blake
545 Sea “Lake” phase would be required.

546 **4.3 Impact of S-Fe-CH₄ dynamics on sedimentary P diagenesis**

547 Degradation of organic matter and the subsequent release of HPO₄²⁻ to the pore water during early diagenesis
548 typically results in a sink-switching from organic P to authigenic P-bearing phases such as Ca phosphates (Filippelli,
549 1997; Ruttenger and Berner, 1993; Slomp et al., 1996b), Mn-Ca carbonates (Jilbert and Slomp, 2013; Mort et al.,
550 2010; Suess, 1979) or reduced Fe phosphates (Burns, 1997; Jilbert and Slomp, 2013; Martens et al., 1978; März et
551 al., 2008). Reductive dissolution of Fe oxides by dissolved sulfide and the following liberation of HPO₄²⁻ may also
552 contribute to the buildup of pore water HPO₄²⁻ (Burns, 1997; Egger et al., 2015a; März et al., 2008; Schulz et al.,
553 1994). Thus, the downward sulfidization ultimately results in the accumulation of dissolved HPO₄²⁻ in the pore water
554 as the sulfidization front moves downward into the limnic deposits (Fig. 7).

555 The pore water profile of HPO₄²⁻ (Fig. 3) indicates the presence of a sink for HPO₄²⁻ below the sulfidization front
556 and, to a lesser extent, in the sulfidic sediments around the SMTZ, likely unrelated to Ca-P authigenesis (Fig. 5).
557 Such a sink for HPO₄²⁻ below sulfidic sediments has been observed previously (Burns, 1997; Egger et al., 2015a;
558 März et al., 2008; Schulz et al., 1994; Slomp et al., 2013) and shown to be most likely the result of vivianite
559 formation (Egger et al., 2015a; Hsu et al., 2014; März et al., 2008). Abundant dissolved Fe²⁺ and a peak in Fe-
560 associated P below the sulfidization front observed in this study (Fig. 3 and Fig. 5) suggest that vivianite authigenesis
561 might also be occurring in the limnic deposits below the sulfidization front in Black Sea sediments.

562 Assuming that vivianite formation represents the only sink for pore water HPO₄²⁻ results in a good fit between the
563 modeled and measured pore water profile of HPO₄²⁻ below the sulfidization front (Fig. 3). Modeled vivianite

564 formation accounts for up to 70 % of total Fe-associated P directly below the sulfidization front. However, the model
565 underestimates the sharp peak in Fe-associated P directly below the sulfidization front, suggesting that modeled
566 vivianite formation likely underestimates the actual contribution of vivianite in these sediments. In the limnic
567 deposits not yet impacted by the downward sulfidization, modeled vivianite accounts for ~ 20 – 30 % of total Fe-
568 associated P. From this, we estimate that vivianite may be responsible for > 20 % of total P burial directly below the
569 sulfidization front and for ~ 10 % of total P burial in the deep limnic deposits at depth.

570 Running the model without Fe-AOM and thus without Fe reduction at depth results in modeled pore water HPO_4^{2-}
571 concentrations of up to ~ 350 μM at depth in the sediment (Fig. 8). This suggests that Fe-AOM can promote
572 conditions that allow sequestration of a significant proportion of P as vivianite in the limnic deposits below the
573 sulfidization front. Consistent with earlier findings, Fe-AOM likely only accounts for a small fraction of total CH_4
574 oxidation, but may substantially impact the biogeochemical cycling of sedimentary P (Egger et al., 2015a, 2015b;
575 Rooze et al., 2016).

576 The deviation between the modeled and measured profiles of HPO_4^{2-} and Fe-associated P in the upper 300 cm of
577 sediment (Fig. 3 and Fig. 5) could indicate apatite authigenesis (Dijkstra et al., 2014) or the formation of vivianite in
578 microenvironments as previously suggested for sulfidic sediments (Dijkstra et al., 2014; Jilbert and Slomp, 2013).

579 For example, *Deltaproteobacteria*, known to be involved in SO_4 -AOM, have been shown to accumulate Fe- and P-
580 rich inclusions in their cells (Milucka et al., 2012). They may therefore provide a potential explanation for the
581 occurrence of Fe-associated P in sulfidic sediments (Dijkstra et al., 2014; Jilbert and Slomp, 2013). However, such
582 microenvironments are not captured in our model.

583 In the diagenetic model, vivianite undergoes dissolution if sulfide is present in the pore waters (Table 3). Sulfide-
584 induced vivianite dissolution significantly improved the model fit to the measured HPO_4^{2-} and sulfide data. With the
585 downward migration of dissolved sulfide, modeled vivianite becomes increasingly enriched below the sulfidization
586 front (Fig. 7). Thus, similar to the sulfidization front, a downward diffusive vivianite front may exist in sedimentary
587 systems experiencing downward sulfidization.

588 In summary, the enhanced downward sulfidization driven by SO_4 -AOM leads to dissolution of Fe oxide-bound P in
589 the lake deposits. Below the sulfidization front, downward diffusing HPO_4^{2-} is bound again in authigenic vivianite
590 due to high concentrations of dissolved Fe^{2+} at depth in the sediment generated by ongoing Fe oxide reduction. As a
591 result, trends in total P with depth are significantly altered, showing an accumulation in total P below the
592 sulfidization front unrelated to changes in organic matter deposition and enhanced sedimentary P burial during
593 deposition.

594 5. Conclusions

595 In the Black Sea, the shift from a freshwater lake to a marine system and subsequent downward diffusion of marine
596 SO_4^{2-} into the CH_4 -bearing lake sediments results in a multitude of diagenetic reactions around the SMTZ (Fig. 9).
597 The diagenetic model developed in this study shows that SO_4 -AOM within the SMTZ significantly enhances the
598 downward diffusive flux of sulfide into the deep limnic deposits, forming a distinct diagenetic sulfidization front
599 around 300 cm depth in the sediment. Our results indicate that without this additional source of dissolved sulfide in

600 the SMTZ, the current sulfidization front would be located around a depth of 150 cm. During the downward
601 sulfidization, Fe oxides, Fe carbonates and vivianite are converted to Fe sulfide phases, leading to an enrichment in
602 solid phase S contents and the release of HPO_4^{2-} to the pore water. Our results further support the hypothesis that part
603 of the downward migrating sulfide is re-oxidized to SO_4^{2-} upon reaction with ferric Fe minerals, fueling a cryptic S
604 cycle and thus stimulating slow rates ($\sim 1\text{-}5 \text{ pmol cm}^{-3} \text{ d}^{-1}$) of SO_4 -AOM in the SO_4^{2-} -depleted limnic deposits below
605 the SMTZ (Holmkvist et al., 2011a, 2011b; Knab et al., 2009; Leloup et al., 2007).

606 We propose that besides organoclastic Fe oxide reduction and reactivation of less reactive Fe oxides by
607 methanogens, AOM coupled to the reduction of Fe oxides may also be a possible mechanism explaining the high
608 concentrations of Fe^{2+} in the pore water below the sulfidization front. The buildup of dissolved Fe^{2+} at depth creates
609 conditions that allow sequestration of the downward diffusing HPO_4^{2-} as authigenic vivianite, resulting in an
610 accumulation of total P in these sediments.

611 The diagenetic processes described here reveal that AOM may strongly overprint burial records of Fe, S and P in
612 depositional marine systems subject to changes in organic matter loading or water column salinity such as coastal
613 environments (Egger et al., 2015a; Rooze et al., 2016), deep-sea fan sediments (März et al., 2008; Schulz et al.,
614 1994) and many high-latitude seas (Holmkvist et al., 2014; Treude et al., 2014). Interpreting these diagenetic patterns
615 as primary sedimentary signals may lead to incorrect reconstructions of environmental conditions during sediment
616 deposition.

617 **Acknowledgements**

618 We thank the captain, crew and shipboard party of the PHOXY cruise aboard R/V Pelagia to the Black Sea in June
619 2013 and G. J. Reichart. We also thank NIOZ Marine Research Facilities for their support and K. Bakker and S.
620 Ossebaar for their contribution to the pore water analysis. D. van de Meent, T. Claessen, T. Zalm, A. van Dijk, E.
621 Dekker and G. Megens are acknowledged for technical and analytical assistance in Utrecht and M. Hagens for her
622 support with the modelling. We further thank C. van der Veen for the methane isotope analysis. This research was
623 funded by ERC Starting Grant 278364, NWO Open Competition Grant 822.01013 and NWO-Vici Grant 865.13.005
624 (to C. P. Slomp). In addition, P. Kraal would like to acknowledge NWO Veni grant 863.14.014. This work was
625 carried out under the program of the Netherlands Earth System Science Centre (NESSC), financially supported by
626 the Ministry of Education, Culture and Science (OCW). Orit Sivan, Wei-Li Hong and an anonymous reviewer are
627 gratefully acknowledged for their insightful comments and suggestions that improved the quality of the manuscript.
628

629 **References**

630 Achtnich, C., Bak, F. and Conrad, R.: Competition for electron donors among nitrate reducers, ferric iron reducers,
631 sulfate reducers, and methanogens in anoxic paddy soil, *Biol. Fertil. Soils*, 19, 65–72, doi:10.1007/BF00336349,
632 1995.

633 Alperin, M. J., Reeburgh, W. S. and Whiticar, M. J.: Carbon and hydrogen isotope fractionation resulting from

634 anaerobic methane oxidation, *Glob. Biogeochem. Cycl.*, 2(3), 279–288, doi:10.1029/GB002i003p00279, 1988.

635 Amos, R. T., Bekins, B. A., Cozzarelli, I. M., Voytek, M. A., Kirshtein, J. D., Jones, E. J. P. and Blowes, D. W.:
636 Evidence for iron-mediated anaerobic methane oxidation in a crude oil-contaminated aquifer, *Geobiology*, 10(6),
637 506–17, doi:10.1111/j.1472-4669.2012.00341.x, 2012.

638 Arthur, M. A. and Dean, W. E.: Organic-matter production and evolution of anoxia in the Holocene Black Sea,
639 *Paleoceanography*, 13(4), 395–411, doi:10.1029/98PA01161, 1998.

640 Beal, E. J., House, C. H. and Orphan, V. J.: Manganese- and iron-dependent marine methane oxidation, *Science* (80-
641), 325, 184–187, doi:10.1126/science.1169984, 2009.

642 Berg, P., Rysgaard, S. and Thamdrup, B.: Dynamic modeling of early diagenesis and nutrient cycling. A case study
643 in an Arctic marine sediment, *Am. J. Sci.*, 303(10), 905–955, doi:10.2475/ajs.303.10.905, 2003.

644 Berner, R. A.: Iron sulfides in Pleistocene deep Black Sea sediments and their paleo-oceanographic significance, in
645 *The Black Sea - Geology, Chemistry and Biology*, edited by E. T. Degens and D. A. Ross, pp. 524–531, Plenum
646 Press., 1974.

647 Berner, R. A.: *Early Diagenesis: A Theoretical Approach*, Princeton University Press., 1980.

648 Bodegom, P. M., Scholten, J. C. M. and Stams, A. J. M.: Direct inhibition of methanogenesis by ferric iron, *FEMS*
649 *Microbiol. Ecol.*, 49(2), 261–268, doi:10.1016/j.femsec.2004.03.017, 2004.

650 Bond, D. R. and Lovley, D. R.: Reduction of Fe(III) oxide by methanogens in the presence and absence of
651 extracellular quinones, *Environ. Microbiol.*, 4(2), 115–24, doi:10.1046/j.1462-2920.2002.00279.x, 2002.

652 Boudreau, B. P.: The diffusive tortuosity of fine-grained unlithified sediments, *Geochim. Cosmochim. Acta*, 60(16),
653 3139–3142, doi:10.1016/0016-7037(96)00158-5, 1996.

654 Boudreau, B. P.: *Diagenetic models and their implementation. Modelling transport and reactions in aquatic*
655 *sediments*, Springer., 1997.

656 Brass, M. and Röckmann, T.: Continuous-flow isotope ratio mass spectrometry method for carbon and hydrogen
657 isotope measurements on atmospheric methane, *Atmos. Meas. Tech.*, 3(6), 1707–1721, doi:10.5194/amt-3-1707-
658 2010, 2010.

659 Burns, S. J.: Early diagenesis in Amazon fan sediments, in *Proceeding of the Ocean Drilling Program, Scientific*
660 *Results*, vol. 155, edited by R. D. Flood, D. J. W. Piper, A. Klaus, and L. C. Peterson, pp. 497–504., 1997.

661 Burton, E. D., Sullivan, L. A., Bush, R. T., Johnston, S. G. and Keene, A. F.: A simple and inexpensive chromium-
662 reducible sulfur method for acid-sulfate soils, *Appl. Geochemistry*, 23(9), 2759–2766,
663 doi:10.1016/j.apgeochem.2008.07.007, 2008.

664 Capet, A., Beckers, J.-M. and Grégoire, M.: Drivers, mechanisms and long-term variability of seasonal hypoxia on
665 the Black Sea northwestern shelf – is there any recovery after eutrophication?, *Biogeosciences*, 10, 3943–3962,
666 doi:10.5194/bg-10-3943-2013, 2013.

667 Chanton, J., Chaser, L., Glasser, P. and Siegel, D.: Carbon and hydrogen isotopic effects in microbial methane from

668 terrestrial environments, in *Stable isotopes and biosphere-atmosphere interactions*, edited by L. Flanagan, pp. 85–
669 105, Elsevier-Academic Press., Amsterdam., 2005.

670 Chanton, J. P.: The effect of gas transport on the isotope signature of methane in wetlands, *Org. Geochem.*, 36, 753–
671 768, doi:10.1016/j.orggeochem.2004.10.007, 2005.

672 Claff, S. R., Sullivan, L. A., Burton, E. D. and Bush, R. T.: A sequential extraction procedure for acid sulfate soils:
673 Partitioning of iron, *Geoderma*, 155(3-4), 224–230, doi:10.1016/j.geoderma.2009.12.002, 2010.

674 Crowe, S. A., Katsev, S., Leslie, K., Sturm, A., Magen, C., Nomosatryo, S., Pack, M. A., Kessler, J. D., Reeburgh,
675 W. S., Roberts, J. A., González, L., Douglas Haffner, G., Mucci, A., Sundby, B. and Fowle, D. A.: The methane
676 cycle in ferruginous Lake Matano, *Geobiology*, 9(1), 61–78, doi:10.1111/j.1472-4669.2010.00257.x, 2011.

677 Cruz Viggi, C., Rossetti, S., Fazi, S., Paiano, P., Majone, M. and Aulenta, F.: Magnetite particles triggering a faster
678 and more robust syntrophic pathway of methanogenic propionate degradation, *Environ. Sci. Technol.*, 48(13), 7536–
679 7543, doi:10.1021/es5016789, 2014.

680 Degens, E. T. and Ross, D. A.: *The Black Sea - geology, chemistry, and biology*: American Association of
681 Petroleum Geologists Memoir 20., 1974.

682 Dijkstra, N., Kraal, P., Kuypers, M. M. M., Schnetger, B. and Slomp, C. P.: Are iron-phosphate minerals a sink for
683 phosphorus in anoxic Black Sea sediments?, *PLoS One*, 9(7), doi:10.1371/journal.pone.0101139, 2014.

684 Eckert, S., Brumsack, H.-J., Severmann, S., Schnetger, B., März, C. and Frollje, H.: Establishment of euxinic
685 conditions in the Holocene Black Sea, *Geology*, 41(4), 431–434, 2013.

686 Egger, M., Jilbert, T., Behrends, T., Rivard, C. and Slomp, C. P.: Vivianite is a major sink for phosphorus in
687 methanogenic coastal surface sediments, *Geochim. Cosmochim. Acta*, 169, 217–235, doi:10.1016/j.gca.2015.09.012,
688 2015a.

689 Egger, M., Rasigraf, O., Sapart, C. J., Jilbert, T., Jetten, M. S. M., Röckmann, T., van der Veen, C., Bândă, N.,
690 Kartal, B., Ettwig, K. F. and Slomp, C. P.: Iron-mediated anaerobic oxidation of methane in brackish coastal
691 sediments, *Environ. Sci. Technol.*, 49(1), 277–283, doi:10.1021/es503663z, 2015b.

692 Ettwig, K. F., Butler, M. K., Le Paslier, D., Pelletier, E., Mangenot, S., Kuypers, M. M. M., Schreiber, F., Dutilh, B.
693 E., Zedelius, J., de Beer, D., Gloerich, J., Wessels, H. J. C. T., van Alen, T., Luesken, F., Wu, M. L., van de Pas-
694 Schoonen, K. T., Op den Camp, H. J. M., Janssen-Megens, E. M., Francoijs, K.-J., Stunnenberg, H., Weissenbach, J.,
695 Jetten, M. S. M. and Strous, M.: Nitrite-driven anaerobic methane oxidation by oxygenic bacteria, *Nature*, 464, 543–
696 548, doi:10.1038/nature08883, 2010.

697 Filippelli, G. M.: Controls on phosphorus concentration and accumulation in oceanic sediments, *Mar. Geol.*, 139(1–
698 4), 231–240, 1997.

699 Froelich, P. N., Klinkhammer, G. P., Bender, M. L., Luedtke, N. A., Heath, G. R., Cullen, D., Dauphin, P.,
700 Hammond, D., Hartman, B. and Maynard, V.: Early oxidation of organic matter in pelagic sediments of the eastern
701 equatorial Atlantic: suboxic diagenesis, *Geochim. Cosmochim. Acta*, 43(7), 1075–1090, doi:10.1016/0016-
702 7037(79)90095-4, 1979.

703 Grasshoff, K.: A simultaneous multiple channel system for nutrient analysis in seawater with analog and digital data
704 record, *Contrib. 2338*, Woods Hole, 1969.

705 Happell, J. D., Chanton, J. P. and Showers, W. J.: Methane transfer across the water-air interface in stagnant wooded
706 swamps of Florida : Evaluation of mass-transfer coefficients and isotopic fractionation, , 40(2), 290–298, 1995.

707 Henkel, S., Mogollón, J. M., Nöthen, K., Franke, C., Bogus, K., Robin, E., Bahr, A., Blumenberg, M., Pape, T.,
708 Seifert, R., März, C., de Lange, G. J. and Kasten, S.: Diagenetic barium cycling in Black Sea sediments - A case
709 study for anoxic marine environments, *Geochim. Cosmochim. Acta*, 88, 88–105, doi:10.1016/j.gca.2012.04.021,
710 2012.

711 Hindmarsh, A. C.: ODEPACK, a systematized collection of ODE solvers, in *IMACS Transactions on Scientific
712 Computation*, Vol. 1, edited by R. S. Stepleman and Others, pp. 55–64, North-Holland, Amsterdam., 1983.

713 Holler, T., Wegener, G., Knittel, K., Boetius, A., Brunner, B., Kuypers, M. M. M. and Widdel, F.: Substantial (13)
714 C/(12) C and D/H fractionation during anaerobic oxidation of methane by marine consortia enriched in vitro,
715 *Environ. Microbiol. Rep.*, 1(5), 370–6, doi:10.1111/j.1758-2229.2009.00074.x, 2009.

716 Holler, T., Wegener, G., Niemann, H., Ferdelman, T. G., Boetius, A., Kristiansen, T. Z., Molina, H., Pandey, A.,
717 Werner, J. K., Juluri, K. R., Xu, Y., Glenn, D., Parang, K. and Snyder, S. H.: Carbon and sulfur back flux during
718 anaerobic microbial oxidation of methane and coupled sulfate reduction, *Proc. Natl. Acad. Sci.*, 109(51), 21170–
719 21170, doi:10.1073/pnas.1218683109, 2012.

720 Holmkvist, L., Ferdelman, T. G. and Jørgensen, B. B.: A cryptic sulfur cycle driven by iron in the methane zone of
721 marine sediment (Aarhus Bay, Denmark), *Geochim. Cosmochim. Acta*, 75(12), 3581–3599,
722 doi:10.1016/j.gca.2011.03.033, 2011a.

723 Holmkvist, L., Kamyshny, A., Brüchert, V., Ferdelman, T. G. and Jørgensen, B. B.: Sulfidization of lacustrine
724 glacial clay upon Holocene marine transgression (Arkona Basin, Baltic Sea), *Geochim. Cosmochim. Acta*, 142, 75–
725 94, doi:10.1016/j.gca.2014.07.030, 2014.

726 Holmkvist, L., Kamyshny, A., Vogt, C., Vamvakopoulos, K., Ferdelman, T. G. and Jørgensen, B. B.: Sulfate
727 reduction below the sulfate–methane transition in Black Sea sediments, *Deep Sea Res. Part I Oceanogr. Res. Pap.*,
728 58(5), 493–504, doi:10.1016/j.dsr.2011.02.009, 2011b.

729 Hsu, T.-W., Jiang, W.-T. and Wang, Y.: Authigenesis of vivianite as influenced by methane-induced sulfidization in
730 cold-seep sediments off southwestern Taiwan, *J. Asian Earth Sci.*, 89, 88–97, doi:10.1016/j.jseaes.2014.03.027,
731 2014.

732 Ingall, E. D., Bustin, R. M. and Van Cappellen, P.: Influence of water column anoxia on the burial and preservation
733 of carbon and phosphorus in marine shales, *Geochim. Cosmochim. Acta*, 57(2), 303–316, 1993.

734 Jilbert, T. and Slomp, C. P.: Iron and manganese shuttles control the formation of authigenic phosphorus minerals in
735 the euxinic basins of the Baltic Sea, *Geochim. Cosmochim. Acta*, 107, 155–169, doi:10.1016/j.gca.2013.01.005,
736 2013.

737 Jørgensen, B. B.: A comparison of methods for the quantification of bacterial sulfate reduction in coastal marine

738 sediments. II. Calculations from mathematical models, *Geomicrobiol. J.*, 1, 29–51,
739 doi:10.1080/01490457809377721, 1978.

740 Jørgensen, B. B., Böttcher, M. E., Lüschen, H., Neretin, L. N. and Volkov, I. I.: Anaerobic methane oxidation and a
741 deep H₂S sink generate isotopically heavy sulfides in Black Sea sediments, *Geochim. Cosmochim. Acta*, 68(9),
742 2095–2118, doi:10.1016/j.gca.2003.07.017, 2004.

743 Jørgensen, B. B., Weber, A. and Zopfi, J.: Sulfate reduction and anaerobic methane oxidation in Black Sea
744 sediments, *Deep Sea Res. Part I Oceanogr. Res. Pap.*, 48, 2097–2120, doi:10.1016/S0967-0637(01)00007-3, 2001.

745 Kato, S., Hashimoto, K. and Watanabe, K.: Methanogenesis facilitated by electric syntrophy via (semi)conductive
746 iron-oxide minerals, *Environ. Microbiol.*, 14(7), 1646–1654, doi:10.1111/j.1462-2920.2011.02611.x, 2012.

747 Kemp, W. M., Testa, J. M., Conley, D. J., Gilbert, D. and Hagy, J. D.: Temporal responses of coastal hypoxia to
748 nutrient loading and physical controls, *Biogeosciences*, 6(12), 2985–3008, doi:10.5194/bg-6-2985-2009, 2009.

749 Knab, N. J., Cragg, B. A., Hornibrook, E. R. C., Holmkvist, L., Pancost, R. D., Borowski, C., Parkes, R. J. and
750 Jørgensen, B. B.: Regulation of anaerobic methane oxidation in sediments of the Black Sea, *Biogeosciences*, (6),
751 1505–1518, doi:10.5194/bg-6-1505-2009, 2009.

752 Knittel, K. and Boetius, A.: Anaerobic oxidation of methane: progress with an unknown process, *Annu. Rev.*
753 *Microbiol.*, 63, 311–334, doi:10.1146/annurev.micro.61.080706.093130, 2009.

754 Kraal, P. and Slomp, C. P.: Rapid and extensive alteration of phosphorus speciation during oxic storage of wet
755 sediment samples, *PLoS One*, 9(5), e96859, 2014.

756 Kraal, P., Slomp, C. P., Forster, A. and Kuypers, M. M. M.: Pyrite oxidation during sample storage determines
757 phosphorus fractionation in carbonate-poor anoxic sediments, *Geochim. Cosmochim. Acta*, 73(11), 3277–3290,
758 doi:10.1016/j.gca.2009.02.026, 2009.

759 Leloup, J., Fossing, H., Kohls, K., Holmkvist, L., Borowski, C. and Jørgensen, B. B.: Sulfate-reducing bacteria in
760 marine sediment (Aarhus Bay, Denmark): abundance and diversity related to geochemical zonation, *Environ.*
761 *Microbiol.*, 11(5), 1278–1291, doi:10.1111/j.1462-2920.2008.01855.x, 2009.

762 Leloup, J., Loy, A., Knab, N. J., Borowski, C., Wagner, M. and Jørgensen, B. B.: Diversity and abundance of sulfate-
763 reducing microorganisms in the sulfate and methane zones of a marine sediment, Black Sea, *Environ. Microbiol.*,
764 9(1), 131–142, doi:10.1111/j.1462-2920.2006.01122.x, 2007.

765 Li, H., Chang, J., Liu, P., Fu, L., Ding, D. and Lu, Y.: Direct interspecies electron transfer accelerates syntrophic
766 oxidation of butyrate in paddy soil enrichments, *Environ. Microbiol.*, 17, 1–45, doi:10.1111/1462-2920.12576, 2014.

767 Liu, D., Wang, H., Dong, H., Qiu, X., Dong, X. and Cravotta, C. A.: Mineral transformations associated with
768 goethite reduction by *Methanosarcina barkeri*, *Chem. Geol.*, 288(1-2), 53–60, doi:10.1016/j.chemgeo.2011.06.013,
769 2011.

770 Lovley, D. R.: Dissimilatory Fe(III) and Mn(IV) reduction, *Microbiol. Rev.*, 55(2), 259–287, 1991.

771 Lovley, D. R. and Phillips, E. J. P.: Competitive mechanisms for inhibition of sulfate reduction and methane

772 production in the zone of ferric iron reduction in sediments, *Appl. Environ. Microbiol.*, 53(11), 1987.

773 Lovley, D. R., Phillips, E. J. P. and Lonergan, D. J.: Hydrogen and formate oxidation coupled to dissimilatory
774 reduction of iron or manganese by *Alteromonas putrefaciens*, *Appl. Environ. Microbiol.*, 55(3), 700–706, 1989.

775 Martens, C. S., Albert, D. B. and Alperin, M. J.: Stable isotope tracing of anaerobic methane oxidation in the gassy
776 sediments of Eckernförde Bay, German Baltic Sea, *Am. J. Sci.*, 299, 589–610, doi:10.2475/ajs.299.7-9.589, 1999.

777 Martens, C. S., Berner, R. A. and Rosenfeld, J. K.: Interstitial water chemistry of anoxic Long Island Sound
778 sediments. 2. Nutrient regeneration and phosphate removal, *Limnol. Oceanogr.*, 23(4), 605–617, 1978.

779 März, C., Hoffmann, J., Bleil, U., de Lange, G. J. and Kasten, S.: Diagenetic changes of magnetic and geochemical
780 signals by anaerobic methane oxidation in sediments of the Zambezi deep-sea fan (SW Indian Ocean), *Mar. Geol.*,
781 255(3-4), 118–130, doi:10.1016/j.margeo.2008.05.013, 2008.

782 Meysman, F. J. R., Boudreau, B. P. and Middelburg, J. J.: Modeling reactive transport in sediments subject to
783 bioturbation and compaction, *Geochim. Cosmochim. Acta*, 69(14), 3601–3617, doi:10.1016/j.gca.2005.01.004,
784 2005.

785 Milucka, J., Ferdelman, T. G., Polerecky, L., Franzke, D., Wegener, G., Schmid, M., Lieberwirth, I., Wagner, M.,
786 Widdel, F. and Kuypers, M. M. M.: Zero-valent sulphur is a key intermediate in marine methane oxidation, *Nature*,
787 491(7425), 541–6, doi:10.1038/nature11656, 2012.

788 Mogollón, J. M., Dale, A. W., Jensen, J. B., Schlüter, M. and Regnier, P.: A method for the calculation of anaerobic
789 oxidation of methane rates across regional scales: An example from the Belt Seas and The Sound (North Sea-Baltic
790 Sea transition), *Geo-Marine Lett.*, 33(4), 299–310, doi:10.1007/s00367-013-0329-z, 2013.

791 Moodley, L., Middelburg, J. J., Herman, P. M. J., Soetaert, K. and de Lange, G. J.: Oxygenation and organic-matter
792 preservation in marine sediments: Direct experimental evidence from ancient organic carbon-rich deposits, *Geology*,
793 33(11), 889, doi:10.1130/G21731.1, 2005.

794 Mort, H. P., Slomp, C. P., Gustafsson, B. G. and Andersen, T. J.: Phosphorus recycling and burial in Baltic Sea
795 sediments with contrasting redox conditions, *Geochim. Cosmochim. Acta*, 74(4), 1350–1362,
796 doi:10.1016/j.gca.2009.11.016, 2010.

797 Murphy, J. and Riley, J. P.: A modified single solution method for the determination of phosphate in natural waters,
798 *Anal. Chim. Acta*, 27, 31–36, doi:10.1016/S0003-2670(00)88444-5, 1962.

799 Neretin, L. N., Böttcher, M. E., Jørgensen, B. B., Volkov, I. I., Lüschen, H. and Hilgenfeldt, K.: Pyritization
800 processes and greigite formation in the advancing sulfidization front in the Upper Pleistocene sediments of the Black
801 Sea, *Geochim. Cosmochim. Acta*, 68(9), 2081–2093, doi:10.1016/S0016-7037(00)00450-2, 2004.

802 Petzoldt, L. R.: Automatic selection of methods for solving stiff and nonstiff systems of ordinary differential
803 equations, *SIAM J. Sci. Stat. Comput.*, 4, 136–148, doi:10.1137/0904010, 1983.

804 Poulton, S. and Canfield, D.: Development of a sequential extraction procedure for iron: implications for iron
805 partitioning in continentally derived particulates, *Chem. Geol.*, 214(3-4), 209–221,
806 doi:10.1016/j.chemgeo.2004.09.003, 2005.

807 Qu, D., Ratering, S. and Schnell, S.: Microbial reduction of weakly crystalline iron (III) oxides and suppression of
808 methanogenesis in paddy soil, *Bull. Environ. Contam. Toxicol.*, 72(6), 1172–1181, doi:10.1007/s00128-004-0367-3,
809 2004.

810 Raghoebarsing, A. A., Pol, A., van de Pas-Schoonen, K. T., Smolders, A. J. P., Ettwig, K. F., Rijpstra, W. I. C.,
811 Schouten, S., Damsté, J. S. S., Op den Camp, H. J. M., Jetten, M. S. M. and Strous, M.: A microbial consortium
812 couples anaerobic methane oxidation to denitrification, *Nature*, 440(7086), 918–921, doi:10.1038/nature04617, 2006.

813 Raiswell, R. and Canfield, D. E.: The iron biogeochemical cycle past and present, *Geochemical Perspect.*, 1(1),
814 doi:10.7185/geochempersp.1.1, 2012.

815 Rayleigh, J. W. S.: Theoretical considerations respecting the separation of gases by diffusion and similar processes,
816 *Philos. Mag.*, (42), 493–499, 1896.

817 Reeburgh, W.: Oceanic methane biogeochemistry, *Am. Chem. Soc.*, 107(2), 486–513, doi:10.1021/cr050362v, 2007.

818 Reed, D. C., Slomp, C. P. and Gustafsson, B. G.: Sedimentary phosphorus dynamics and the evolution of bottom-
819 water hypoxia: A coupled benthic-pelagic model of a coastal system, *Limnol. Oceanogr.*, 56(3), 1075–1092,
820 doi:10.4319/lo.2011.56.3.1075, 2011a.

821 Reed, D. C., Slomp, C. P. and de Lange, G. J.: A quantitative reconstruction of organic matter and nutrient
822 diagenesis in Mediterranean Sea sediments over the Holocene, *Geochim. Cosmochim. Acta*, 75(19), 5540–5558,
823 doi:10.1016/j.gca.2011.07.002, 2011b.

824 Regnier, P., Dale, A. W., Arndt, S., LaRowe, D. E., Mogollón, J. and Van Cappellen, P.: Quantitative analysis of
825 anaerobic oxidation of methane (AOM) in marine sediments: A modeling perspective, *Earth-Science Rev.*, 106(1-2),
826 105–130, doi:10.1016/j.earscirev.2011.01.002, 2011.

827 Reiche, M., Torburg, G. and Küsel, K.: Competition of Fe(III) reduction and methanogenesis in an acidic fen, *FEMS*
828 *Microbiol. Ecol.*, 65(1), 88–101, doi:10.1111/j.1574-6941.2008.00523.x, 2008.

829 Rickard, D. and Luther, G. W.: Kinetics of pyrite formation by the H₂S oxidation of iron (II) monosulfide in aqueous
830 solutions between 25 and 125°C: The mechanism, *Geochim. Cosmochim. Acta*, 61(1), 135–147, doi:10.1016/S0016-
831 7037(96)00322-5, 1997.

832 Riedinger, N., Formolo, M. J., Lyons, T. W., Henkel, S., Beck, A. and Kasten, S.: An inorganic geochemical
833 argument for coupled anaerobic oxidation of methane and iron reduction in marine sediments, *Geobiology*,
834 doi:10.1111/gbi.12077, 2014.

835 Rooze, J., Egger, M., Tsandev, I. and Slomp, C. P.: Iron-dependent anaerobic oxidation of methane in coastal surface
836 sediments: potential controls and impact, *Limnol. Oceanogr.*, doi:10.1002/lno.10275, 2016.

837 Ruttenberg, K. C.: Development of a sequential extraction method for different forms of phosphorus in marine
838 sediments, *Limnol. Oceanogr.*, 37(7), 1460–1482, 1992.

839 Ruttenberg, K. C. and Berner, R. A.: Authigenic apatite formation and burial in sediments from non-upwelling,
840 continental margin environments, *Geochim. Cosmochim. Acta*, 57(5), 991–1007, doi:10.1016/0016-7037(93)90035-
841 U, 1993.

842 Van Santvoort, P. J. M., De Lange, G. J., Thomson, J., Colley, S., Meysman, F. J. R. and Slomp, C. P.: Oxidation
843 and origin of organic matter in surficial Eastern Mediterranean hemipelagic sediments, *Aquat. Geochemistry*, 8(3),
844 153–175, doi:10.1023/A:1024271706896, 2002.

845 Sapart, C. J., van der Veen, C., Vigano, I., Brass, M., van de Wal, R. S. W., Bock, M., Fischer, H., Sowers, T.,
846 Buizert, C., Sperlich, P., Blunier, T., Behrens, M., Schmitt, J., Seth, B. and Röckmann, T.: Simultaneous stable
847 isotope analysis of methane and nitrous oxide on ice core samples, *Atmos. Meas. Tech.*, 4(12), 2607–2618,
848 doi:10.5194/amt-4-2607-2011, 2011.

849 Scheller, S., Yu, H., Chadwick, G. L., McGlynn, S. E. and Orphan, V. J.: Artificial electron acceptors decouple
850 archaeal methane oxidation from sulfate reduction, *Science* (80-.), 351(6274), 703–707,
851 doi:10.1126/science.aad7154, 2016.

852 Schulz, H. D., Dahmke, A., Schinzel, U., Wallmann, K. and Zabel, M.: Early diagenetic processes, fluxes, and
853 reaction rates in sediments of the South Atlantic, *Geochim. Cosmochim. Acta*, 58(9), 2041–2060, doi:10.1016/0016-
854 7037(94)90284-4, 1994.

855 Segarra, K. E. A., Comerford, C., Slaughter, J. and Joye, S. B.: Impact of electron acceptor availability on the
856 anaerobic oxidation of methane in coastal freshwater and brackish wetland sediments, *Geochim. Cosmochim. Acta*,
857 115, 15–30, doi:10.1016/j.gca.2013.03.029, 2013.

858 Seifert, R., Nauhaus, K., Blumenberg, M., Krüger, M. and Michaelis, W.: Methane dynamics in a microbial
859 community of the Black Sea traced by stable carbon isotopes in vitro, *Org. Geochem.*, 37(10), 1411–1419,
860 doi:10.1016/j.orggeochem.2006.03.007, 2006.

861 Sivan, O., Adler, M., Pearson, A., Gelman, F., Bar-Or, I., John, S. G. and Eckert, W.: Geochemical evidence for
862 iron-mediated anaerobic oxidation of methane, *Limnol. Oceanogr.*, 56(4), 1536–1544,
863 doi:10.4319/lo.2011.56.4.1536, 2011.

864 Sivan, O., Antler, G., Turchyn, A. V., Marlow, J. J. and Orphan, V. J.: Iron oxides stimulate sulfate-driven anaerobic
865 methane oxidation in seeps, *Proc. Natl. Acad. Sci.*, 1–9, doi:10.1073/pnas.1412269111, 2014.

866 Sivan, O., Shusta, S. and Valentine, D. L.: Methanogens rapidly transition from methane production to iron
867 reduction, *Geobiology*, doi:10.1111/gbi.12172, 2016.

868 Slomp, Van der Gaast, S. J. and Van Raaphorst, W.: Phosphorus binding by poorly crystalline iron oxides in North
869 Sea sediments, *Mar. Chem.*, 52(1), 55–73, doi:10.1016/0304-4203(95)00078-X, 1996a.

870 Slomp, C. P., Epping, E. H. G., Helder, W. and Raaphorst, W. Van: A key role for iron-bound phosphorus in
871 authigenic apatite formation in North Atlantic continental platform sediments, *J. Mar. Res.*, 54(6), 1179–1205,
872 doi:10.1357/0022240963213745, 1996b.

873 Slomp, C. P., Mort, H. P., Jilbert, T., Reed, D. C., Gustafsson, B. G. and Wolthers, M.: Coupled dynamics of iron
874 and phosphorus in sediments of an oligotrophic coastal basin and the impact of anaerobic oxidation of methane.,
875 *PLoS One*, 8(4), e62386, doi:10.1371/journal.pone.0062386, 2013.

876 Soetaert, K., Herman, P. M. J. and Middelburg, J. J.: A model of early diagenetic processes from the shelf to abyssal

877 depths, *Geochim. Cosmochim. Acta*, 60(6), 1019–1040, doi:10.1016/0016-7037(96)00013-0, 1996.

878 Soetaert, K. and Meysman, F.: Reactive transport in aquatic ecosystems: Rapid model prototyping in the open source
879 software R, *Environ. Model. Softw.*, 32, 49–60, doi:10.1016/j.envsoft.2011.08.011, 2012.

880 Soetaert, K., Petzoldt, T. and Meysman, F. J. R.: marelac: Tools for Aquatic Sciences. R Package Version 2.1.3,
881 2010.

882 Soulet, G., Delaygue, G., Vallet-Coulomb, C., Böttcher, M. E., Sonzogni, C., Lericolais, G. and Bard, E.: Glacial
883 hydrologic conditions in the Black Sea reconstructed using geochemical pore water profiles, *Earth Planet. Sci. Lett.*,
884 296(1-2), 57–66, doi:10.1016/j.epsl.2010.04.045, 2010.

885 Soulet, G., Ménot, G., Lericolais, G. and Bard, E.: A revised calendar age for the last reconnection of the Black Sea
886 to the global ocean, *Quat. Sci. Rev.*, 30(9-10), 1019–1026, doi:10.1016/j.quascirev.2011.03.001, 2011.

887 Stoll, M. H. C., Bakker, K., Nobbe, G. H. and Haese, R. R.: Continuous-Flow Analysis of Dissolved Inorganic Carbon
888 Content in Seawater, *Anal. Chem.*, 73(17), 4111–4116, doi:10.1021/ac010303r, 2001.

889 Strickland, J. D. and Parsons, T. R.: A Practical Handbook of Seawater Analysis, Bulletin 1., Fisheries Research
890 Board of Canada, Ottawa, Canada., 1972.

891 Suess, E.: Mineral phases formed in anoxic sediments by microbial decomposition of organic matter, *Geochim.*
892 *Cosmochim. Acta*, 43, 339–352, doi:10.1016/0016-7037(79)90199-6, 1979.

893 Thamdrup, B., Roselló-Mora, R. and Amann, R.: Microbial manganese and sulfate reduction in Black Sea shelf
894 sediments, *Appl. Environ. Microbiol.*, 66(2251), 2288–2297, doi:10.1128/AEM.66.7.2888-2897.2000, 2000.

895 Treude, T., Krause, S., Maltby, J., Dale, A. W., Coffin, R. and Hamdan, L. J.: Sulfate reduction and methane
896 oxidation activity below the sulfate-methane transition zone in Alaskan Beaufort Sea continental margin sediments:
897 Implications for deep sulfur cycling, *Geochim. Cosmochim. Acta*, 144, 217–237, doi:10.1016/j.gca.2014.08.018,
898 2014.

899 Vargas, M., Kashefi, K., Blunt-Harris, E. L. and Lovley, D. R.: Microbial evidence for Fe(III) reduction on early
900 Earth, *Nature*, 395, 65–67, doi:10.1038/25720, 1998.

901 Wang, Y. and Van Cappellen, P.: A multicomponent reactive transport model of early diagenesis: Application to
902 redox cycling in coastal marine sediments, *Geochim. Cosmochim. Acta*, 60(16), 2993–3014, doi:10.1016/0016-
903 7037(96)00140-8, 1996.

904 Wankel, S. D., Adams, M. M., Johnston, D. T., Hansel, C. M., Joye, S. B. and Girguis, P. R.: Anaerobic methane
905 oxidation in metalliferous hydrothermal sediments: influence on carbon flux and decoupling from sulfate reduction,
906 *Environ. Microbiol.*, 14(10), 2726–40, doi:10.1111/j.1462-2920.2012.02825.x, 2012.

907 Whiticar, M. J.: Carbon and hydrogen isotope systematics of bacterial formation and oxidation of methane, *Chem.*
908 *Geol.*, 161(1-3), 291–314, doi:10.1016/S0009-2541(99)00092-3, 1999.

909 Yoshinaga, M. Y., Holler, T., Goldhammer, T., Wegener, G., Pohlman, J. W., Brunner, B., Kuypers, M. M. M.,
910 Hinrichs, K. and Elvert, M.: Carbon isotope equilibration during sulphate-limited anaerobic oxidation of methane,

911 Nat. Geosci., 7, 190–194, doi:10.1038/NGEO2069, 2014.

912 Zhou, S., Xu, J., Yang, G. and Zhuang, L.: Methanogenesis affected by the co-occurrence of iron(III) oxides and
913 humic substances, FEMS Microbiol. Ecol., 88(1), 107–120, doi:10.1111/1574-6941.12274, 2014.

914 Zhuang, L., Xu, J., Tang, J. and Zhou, S.: Effect of ferrihydrite biomineralization on methanogenesis in an anaerobic
915 incubation from paddy soil, J. Geophys. Res. Biogeosciences, (120), 876–886, doi:10.1002/2014JG002893, 2015.

916

917

918 **Tables**919 **Table 1. Overview of the sequential P, Fe and S fractionation methods used in this study.**

Step and code	Extractant, extraction time	Target phase
P fractionation (modified from Ruttenberg (1992); done for site 4 (MC & GC) and site 5 (MC & GC))		
1 P_{exch}	1 M MgCl ₂ , pH 8, 0.5 h	Exchangeable P
2^a P_{Fe}	25 g L-1 Na dithionite, pH 7.5, 8 h	Fe-associated P
3^a P_{authi Ca-P}	Na acetate buffer, pH 4, 6 h	P in authigenic and biogenic Ca-P minerals and CaCO ₃
4 P_{detr}	1 M HCl, 24 h	Detrital P
5 P_{org}	Ashing at 550 °C (2h), then 1 M HCl, 24 h	Organic P
Fe fractionation (after Poulton and Canfield (2005); done for site 4 (MC & GC) and site 5 (MC))		
1 Fe_{carb}	1 M Na acetate, pH 4.5, 24 h	Carbonate-associated Fe
2 Fe_{ox1}	1 M hydroxylamine-HCl, 24 h	Amorphous Fe oxides (ferrihydrite)
3 Fe_{ox2}	50 g L-1 Na dithionite, pH 4.8, 2 h	Crystalline Fe oxides (goethite, hematite)
4 Fe_{mag}	0.2 M ammonium oxalate/ 0.17 M oxalic acid, 2 h	Recalcitrant Fe oxides (mostly magnetite)
Fe fractionation (modified from Claff et al. (2010); done for site 4 (MC & GC) and site 5 (MC))		
1 Fe(II)_{HCl}	1 M HCl, 4 h	Labile Fe (carbonates, poorly ordered sulfides)
2 Fe(III)_{HCl}	1 M HCl, 4 h	Labile Fe (easily reducible oxides)
3 Fe(III)_{CDB}	50 g L-1 Na dithionite, pH 4.8, 4 h	Crystalline Fe oxides
4 Fe_{pyrite}	Concentrated HNO ₃ , 2 h	Pyrite (FeS ₂)
S fractionation (after Burton et al. (2008); done for site 4 (MC) and site 5 (MC & GC))		
1 AVS	6 M HCl, 24 h	S in Fe monosulfides (FeS)
2 CRS	Acidic chromous chloride solution, 48 h	S in pyrite (FeS ₂)

920 ^aThese steps were followed by a wash step with 1 M MgCl₂, which was added to the corresponding step. MC = multicore and GC
 921 = gravity core.

922

923 **Table 2. Chemical species included in the diagenetic model.**

Species	Notation	Type
Organic matter ^a	$OM^{\alpha,\beta,\gamma}$	Solid
Iron oxides ^a	$Fe(OH)_3^{\alpha,\beta,\gamma}$	Solid
Iron monosulfide	FeS	Solid
Pyrite	FeS_2	Solid
Siderite	$FeCO_3$	Solid
Elemental sulfur	S_0	Solid
Iron oxide-bound phosphorus	$Fe_{ox}P$	Solid
Vivianite	$Fe_3(PO_4)_2$	Solid
Organic phosphorus	P_{org}	Solid
Authigenic (Ca) phosphorus	CaP	Solid
Detrital phosphorus	$DetrP$	Solid
Chloride	Cl^-	Solute
Oxygen	O_2	Solute
Sulfate	SO_4^{2-}	Solute
Iron	Fe^{2+}	Solute
Hydrogen sulfide ^b	ΣH_2S	Solute
Methane	CH_4	Solute
Ammonium ^b	ΣNH_4^+	Solute
Nitrate	NO_3^-	Solute
Phosphate	ΣHPO_4^{2-}	Solute
Dissolved inorganic carbon	DIC	Solute

924 ^a There are three types of species: reactive (α), less reactive (β) and refractory (γ)

925 ^b Σ denotes that all species of an acid are included

926

927 **Table 3. Reaction pathways and stoichiometries implemented in the diagenetic model.**

Primary redox reactions*	
$OM^{\alpha,\beta} + aO_2 \rightarrow aCO_2 + bNH_4^+ + cH_3PO_4 + aH_2O$	R1
$OM^{\alpha,\beta} + \frac{4a}{5}NO_3^- + \frac{4a}{5}H^+ \rightarrow aCO_2 + bNH_4^+ + cH_3PO_4 + \frac{2a}{5}N_2 + \frac{7a}{5}H_2O$	R2
$OM^{\alpha,\beta} + 4aFe(OH)_3^{\alpha} + 4a\chi^{\alpha}Fe_{ox}P + 12aH^+ \rightarrow aCO_2 + bNH_4^+ + (c + 4a\chi^{\alpha})H_3PO_4 + 4aFe^{2+} + 13aH_2O$	R3
$OM^{\alpha,\beta} + \frac{a}{2}SO_4^{2-} + aH^+ \rightarrow aCO_2 + bNH_4^+ + cH_3PO_4 + \frac{a}{2}H_2S + aH_2O$	R4
$OM^{\alpha,\beta} \rightarrow \frac{a}{2}CO_2 + bNH_4^+ + cH_3PO_4 + \frac{a}{2}CH_4$	R5
$CO_2 + 4H_2 \rightarrow CH_4 + 2H_2O$	R6
Secondary redox and other reaction equations†	
$2O_2 + NH_4^+ + 2HCO_3^- \rightarrow NO_3^- + 2CO_2 + 3H_2O$	R7
$O_2 + 4Fe^{2+} + 8HCO_3^- + 2H_2O + 4\chi^{\alpha}H_2PO_4^- \rightarrow 4Fe(OH)_3^{\alpha} + 4\chi^{\alpha}Fe_{ox}P + 8CO_2$	R8
$2O_2 + FeS \rightarrow SO_4^{2-} + Fe^{2+}$	R9
$7O_2 + 2FeS_2 + 2H_2O \rightarrow 4SO_4^{2-} + 2Fe^{2+} + 4H^+$	R10
$2O_2 + H_2S + 2HCO_3^- \rightarrow SO_4^{2-} + 2CO_2 + 2H_2O$	R11
$2O_2 + CH_4 \rightarrow CO_2 + 2H_2O$	R12
$2Fe(OH)_3^{\alpha} + 2\chi^{\alpha}Fe_{ox}P + H_2S + 4CO_2 \rightarrow 2Fe^{2+} + 2\chi^{\alpha}H_2PO_4^- + S_0 + 4HCO_3^- + 2H_2O$	R13
$2Fe(OH)_3^{\beta} + 2\chi^{\beta}Fe_{ox}P + H_2S + 4CO_2 \rightarrow 2Fe^{2+} + 2\chi^{\beta}H_2PO_4^- + S_0 + 4HCO_3^- + 2H_2O$	R14
$Fe^{2+} + H_2S \rightarrow FeS + 2H^+$	R15
$FeS + H_2S \rightarrow FeS_2 + H_2$	R16
$4S_0 + 4H_2O \rightarrow 3H_2S + SO_4^{2-} + 2H^+$	R17
$FeS + S_0 \rightarrow FeS_2$	R18
$SO_4^{2-} + CH_4 + CO_2 \rightarrow 2HCO_3^- + H_2S$	R19
$CH_4 + 8Fe(OH)_3^{\alpha,\beta} + 8\chi^{\alpha,\beta}Fe_{ox}P + 15H^+ \rightarrow HCO_3^- + 8Fe^{2+} + 8\chi^{\alpha,\beta}H_2PO_4^- + 21H_2O$	R20
$Fe(OH)_3^{\alpha} + (\chi^{\alpha} - \chi^{\beta})Fe_{ox}P \rightarrow Fe(OH)_3^{\beta} + (\chi^{\alpha} - \chi^{\beta})H_2PO_4^-$	R21
$Fe(OH)_3^{\beta} + (\chi^{\beta} - \chi^{\gamma})Fe_{ox}P \rightarrow Fe(OH)_3^{\gamma} + (\chi^{\beta} - \chi^{\gamma})H_2PO_4^-$	R22
$3Fe^{2+} + 2HPO_4^{2-} \rightarrow Fe_3(PO_4)_2 + 2H^+$	R23
$Fe^{2+} + CO_3^{2-} \rightarrow FeCO_3$	R24
$FeCO_3 + H_2S \rightarrow FeS + HCO_3^- + H^+$	R25
$Fe_3(PO_4)_2 + 3H_2S \rightarrow 3FeS + 2HPO_4^{2-} + 4H^+$	R26

928 * Organic matter (OM) is of the form $(CH_2O)_a(NH_4^+)_b(H_3PO_4)_c$, with 'a'=1, 'b' = 1/16 and 'c' = 1/106. Under anoxic bottom
 929 water conditions, 'c' reduces to 0.25 to account for the preferential regeneration of P (e.g. Ingall et al. (1993)). † $\chi^{\alpha,\beta,\gamma}$ refers to
 930 the P:Fe ratio of $Fe(OH)_3^{\alpha,\beta,\gamma}$ (see Supplementary Table S1). **R6 = CH₄ production from DIC (i.e. CO₂); R7 = nitrification; R8 =**
 931 **Fe(OH)₃ formation; R9 = FeS oxidation; R10 = FeS₂ oxidation; R11 = H₂S oxidation; R12 = aerobic CH₄ oxidation; R13 and R14**
 932 **= Fe(OH)₃ reduction by H₂S; R15= FeS formation; R16 = pyrite formation (H₂S pathway); R17 = S₀ disproportionation; R18 =**
 933 **pyrite formation (polysulfide pathway); R19 = SO₄-AOM; R20 = Fe-AOM; R21 = conversion (i.e. crystallization) from α to β**
 934 **phase; R22 = crystallization from β to γ phase; R23 = vivianite formation; R24 = siderite precipitation; R25 = conversion from**
 935 **siderite to FeS; R26 = vivianite dissolution by dissolved sulfide**

936

Primary redox reaction equations	
$R_1 = k_{\alpha,\beta} OM^{\alpha,\beta} \left(\frac{[O_2]}{K_{O_2} + [O_2]} \right)$	(E1)
$R_2 = k_{\alpha,\beta} OM^{\alpha,\beta} \left(\frac{[NO_3^-]}{K_{NO_3^-} + [NO_3^-]} \right) \left(\frac{K_{O_2}}{K_{O_2} + [O_2]} \right)$	(E2)
$R_3 = k_{\alpha,\beta} OM^{\alpha,\beta} \left(\frac{[Fe(OH)_3^{\alpha}]}{K_{Fe(OH)_3^{\alpha}} + [Fe(OH)_3^{\alpha}]} \right) \left(\frac{K_{NO_3^-}}{K_{NO_3^-} + [NO_3^-]} \right) \left(\frac{K_{O_2}}{K_{O_2} + [O_2]} \right)$	(E3)
$R_4 = \Psi k_{\alpha,\beta} OM^{\alpha,\beta} \left(\frac{[SO_4^{2-}]}{K_{SO_4^{2-}} + [SO_4^{2-}]} \right) \left(\frac{K_{Fe(OH)_3^{\alpha}}}{K_{Fe(OH)_3^{\alpha}} + [Fe(OH)_3^{\alpha}]} \right) \left(\frac{K_{NO_3^-}}{K_{NO_3^-} + [NO_3^-]} \right) \left(\frac{K_{O_2}}{K_{O_2} + [O_2]} \right)$	(E4)
$R_5 = \Psi k_{\alpha,\beta} OM^{\alpha,\beta} \left(\frac{K_{SO_4^{2-}}}{K_{SO_4^{2-}} + [SO_4^{2-}]} \right) \left(\frac{K_{Fe(OH)_3^{\alpha}}}{K_{Fe(OH)_3^{\alpha}} + [Fe(OH)_3^{\alpha}]} \right) \left(\frac{K_{NO_3^-}}{K_{NO_3^-} + [NO_3^-]} \right) \left(\frac{K_{O_2}}{K_{O_2} + [O_2]} \right)$	(E5)
$R_6 = k_1 DIC \left(\frac{K_{SO_4^{2-}}}{K_{SO_4^{2-}} + [SO_4^{2-}]} \right) \left(\frac{K_{Fe(OH)_3^{\alpha}}}{K_{Fe(OH)_3^{\alpha}} + [Fe(OH)_3^{\alpha}]} \right) \left(\frac{K_{NO_3^-}}{K_{NO_3^-} + [NO_3^-]} \right) \left(\frac{K_{O_2}}{K_{O_2} + [O_2]} \right)$	(E6)
Secondary redox and other reaction equations	
$R_7 = k_2 [O_2] [NH_4^+]$	(E7)
$R_8 = k_3 [O_2] [Fe^{2+}]$	(E8)
$R_9 = k_4 [O_2] [FeS]$	(E9)
$R_{10} = k_5 [O_2] [FeS_2]$	(E10)
$R_{11} = k_6 [O_2] [\Sigma H_2S]$	(E11)
$R_{12} = k_7 [O_2] [CH_4]$	(E12)
$R_{13} = k_8 [Fe(OH)_3^{\alpha}] [\Sigma H_2S]$	(E13)
$R_{14} = k_9 [Fe(OH)_3^{\beta}] [\Sigma H_2S]$	(E14)
$R_{15} = k_{10} [Fe^{2+}] [\Sigma H_2S]$	(E15)
$R_{16} = k_{11} [FeS] [\Sigma H_2S]$	(E16)
$R_{17} = k_{12} [S_0]$	(E17)
$R_{18} = k_{13} [FeS] [S_0]$	(E18)
$R_{19} = k_{14} [SO_4^{2-}] [CH_4]$	(E19)
$R_{20} = k_{15} [Fe(OH)_3^{\alpha,\beta}] [CH_4]$	(E20)
$R_{21} = k_{16} [Fe(OH)_3^{\alpha}]$	(E21)
$R_{22} = k_{17} [Fe(OH)_3^{\beta}]$	(E22)
$R_{23} = k_{18} [Fe^{2+}] [HPO_4^{2-}]$	(E23)
$R_{24} = k_{19} [Fe^{2+}] [DIC]$	(E24)
$R_{25} = k_{20} [FeCO_3] [\Sigma H_2S]$	(E25)
$R_{26} = k_{21} [Fe_3(PO_4)_2] [\Sigma H_2S]$	(E26)

941 **Table 5. Reaction parameters used in the diagenetic model.**

Parameter	Symbol	Value	Units	Values given in literature
Decay constant for OM ^a	k_{α}	0.05	yr ⁻¹	0.05-1.62 ^{a,b}
Decay constant for OM ^b	k_{β}	0.0086	yr ⁻¹	0.0086 ^b
Limiting concentration of O ₂	K_{O_2}	0.02	mM	0.001-0.03 ^c
Limiting concentration of NO ₃ ⁻	$K_{NO_3^-}$	0.004	mM	0.004-0.08 ^c
Limiting concentration of Fe(OH) ₃	$K_{Fe(OH)_3}$	65	μmol g ⁻¹	65-100 ^c
Limiting concentration of SO ₄ ²⁻	$K_{SO_4^{2-}}$	1.6	mM	1.6 ^c
Attenuation factor for SO ₄ ²⁻ and methanogenesis	Ψ	0.0042	-	0.00157-0.075 ^{b,d}
Rate constant for reaction E6	k_1	0.0011	yr ⁻¹	
Rate constant for reaction E7	k_2	10'000	mM ⁻¹ yr ⁻¹	5'000-39'000 ^{c,d}
Rate constant for reaction E8	k_3	140'000	mM ⁻¹ yr ⁻¹	140'000 ^c
Rate constant for reaction E9	k_4	300	mM ⁻¹ yr ⁻¹	300 ^c
Rate constant for reaction E10	k_5	1	mM ⁻¹ yr ⁻¹	1 ^c
Rate constant for reaction E11	k_6	160	mM ⁻¹ yr ⁻¹	≥ 160 ^c
Rate constant for reaction E12	k_7	10'000'000	mM ⁻¹ yr ⁻¹	10'000'000 ^c
Rate constant for reaction E13	k_8	9.5	mM ⁻¹ yr ⁻¹	≤ 100 ^c
Rate constant for reaction E14	k_9	0.95	mM ⁻¹ yr ⁻¹	Model constrained
Rate constant for reaction E15	k_{10}	150	mM ⁻¹ yr ⁻¹	100-14'800 ^{b,d}
Rate constant for reaction E16	k_{11}	0.0003	mM ⁻¹ yr ⁻¹	3.15 ^e
Rate constant for reaction E17	k_{12}	3	yr ⁻¹	3 ^f
Rate constant for reaction E18	k_{13}	1	mM ⁻¹ yr ⁻¹	7 ^f
Rate constant for reaction E19	k_{14}	0.14	mM ⁻¹ yr ⁻¹	10 ^c
Rate constant for reaction E20	k_{15}	0.00000016	mM ⁻¹ yr ⁻¹	0.0074 ^g
Rate constant for reaction E21	k_{16}	0.6	yr ⁻¹	0.6 ^f
Rate constant for reaction E22	k_{17}	0.000013	yr ⁻¹	Model constrained
Rate constant for reaction E23	k_{18}	0.052	mM ⁻¹ yr ⁻¹	Model constrained
Rate constant for reaction E24	k_{19}	0.0027	mM ⁻¹ yr ⁻¹	Model constrained
Rate constant for reaction E25	k_{20}	0.0008	mM ⁻¹ yr ⁻¹	Model constrained
Rate constant for reaction E26	k_{21}	0.0008	mM ⁻¹ yr ⁻¹	Model constrained

942 ^a Moodley et al. (2005); ^b Reed et al. (2011a); ^c Wang and Van Cappellen (1996); ^d Reed et al. (2011b); ^e Rickard and Luther
 943 (1997); ^f Berg et al. (2003); ^g Rooze et al. (2016)

944
 945
 946

947 **Table 6.** Depth-integrated rates of key processes for selected depth intervals in $\mu\text{mol m}^{-2} \text{d}^{-1}$.

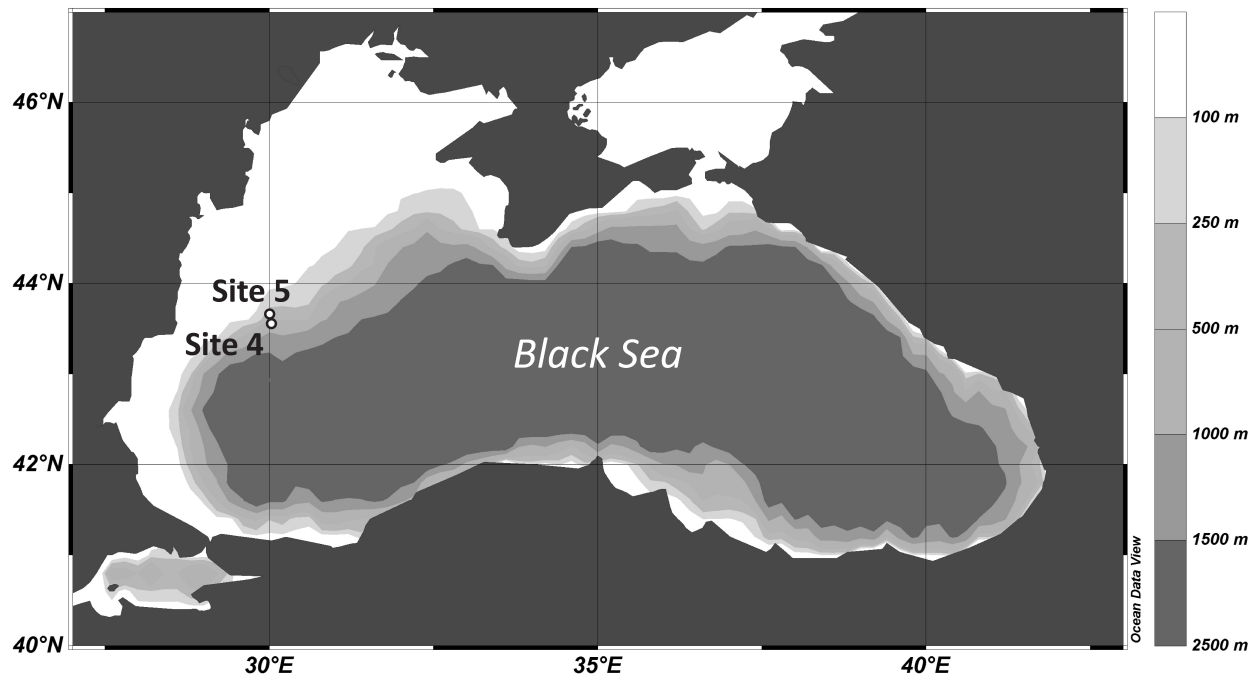
Process	0 – 90 cm ^a	90 - 300 cm ^b	300 – 800 cm ^c	0 – 800 cm
Organoclastic SO_4^{2-} reduction ^d	68.9	5.3	0.003	74.2
CH_4 production ^{e,f}	10.21	37.7	91.8	139.8
SO_4 - AOM	9.4	151.6	1.2	162.2
Fe – AOM ^e	0	0	1.2	1.2
S_0 disproportionation	0	0	0.9	0.9

948 ^a Marine deposits ; ^b limnic sediments around the SMTZ with dissolved sulfide; ^c non-sulfidic limnic deposits; ^d per mol of SO_4^{2-} ; ^e
 949 per mol of CH_4 ; ^f sum of CH_4 production from organic matter and from DIC (i.e. CO_2)

950

951

952

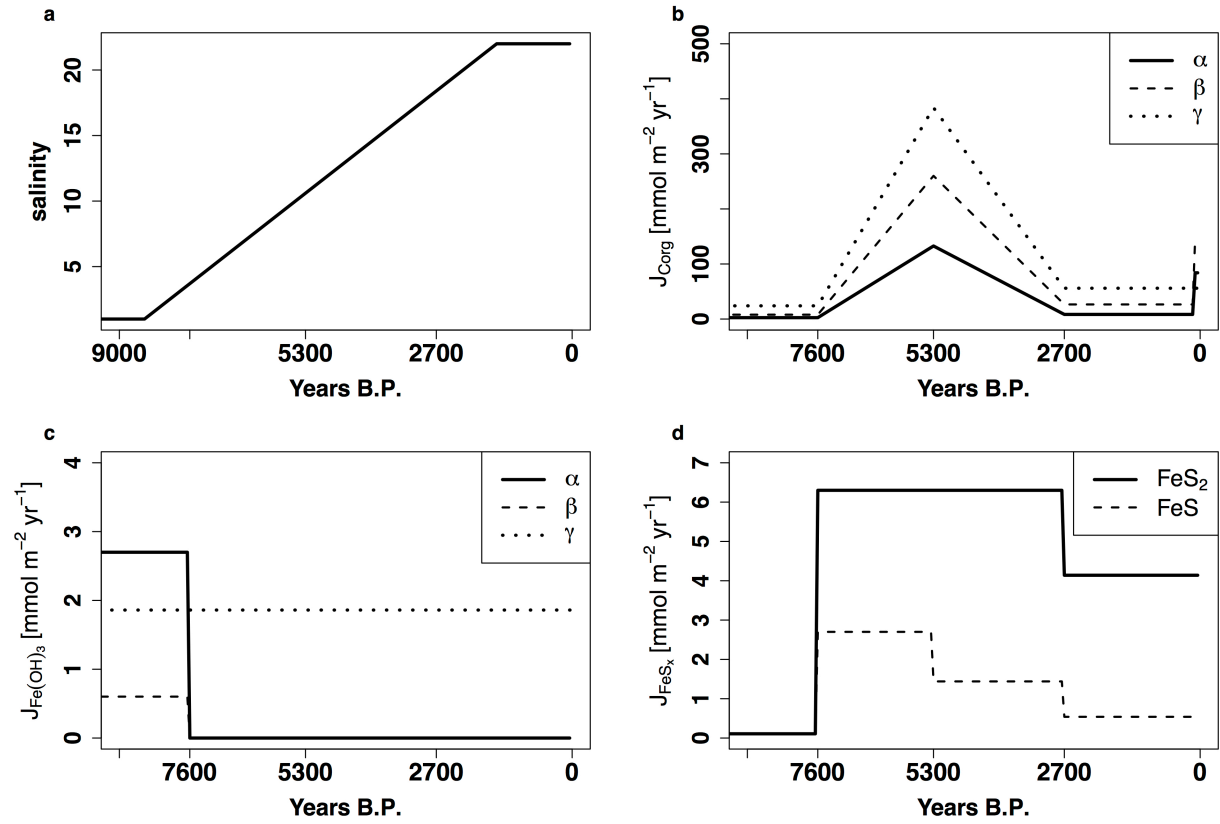


954

955 **Figure 1.** Map showing the locations of site 4 (43°40.6' N, 30°7.5' E; 377 mbss) and site 5 (43°42.6' N, 30°6.1' E; 178 mbss),
956 sampled in June 2013.

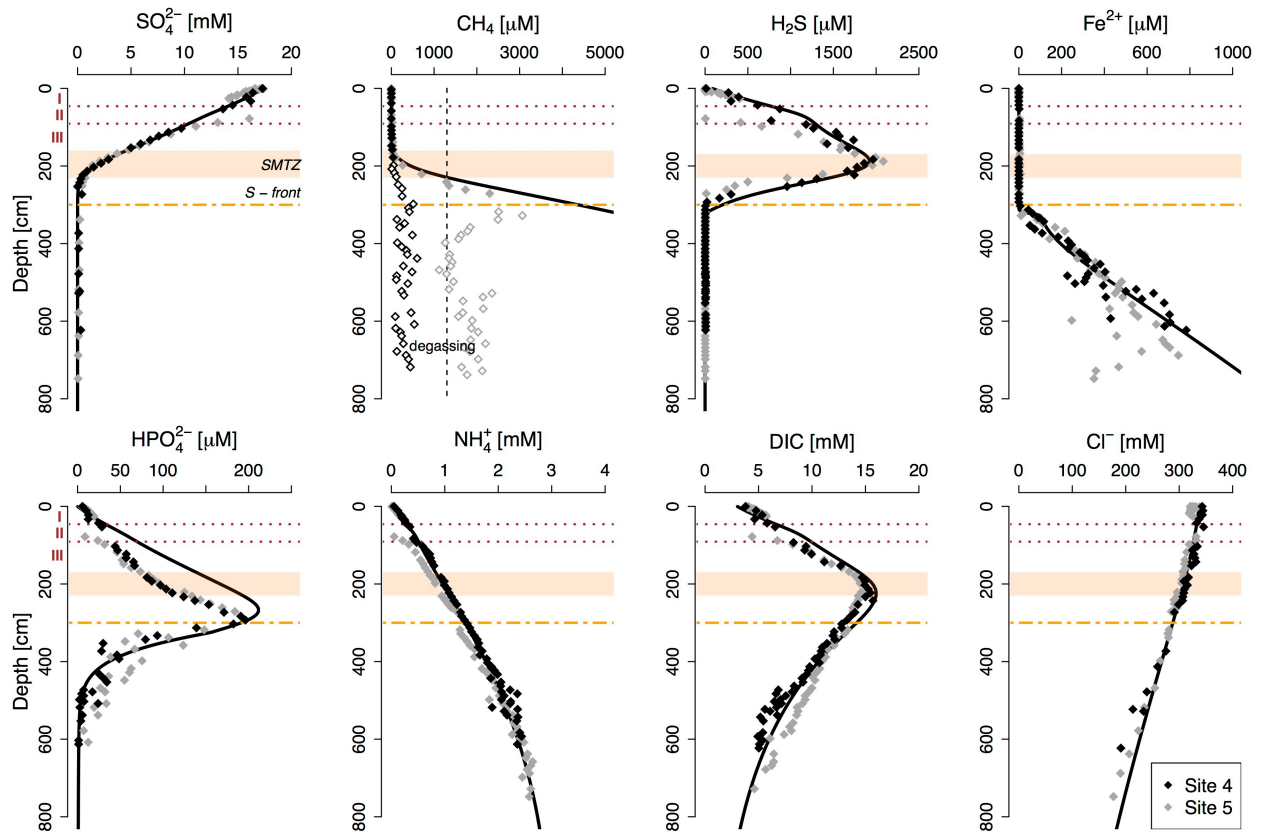
957

958



959
 960 **Figure 2.** Transient evolution of salinity with a linear increase from 1 to 22 between 8500 and 1500 years B.P. (a), fluxes of
 961 organic matter ($J_{\text{C}_{\text{org}}}$; b), Fe oxides ($J_{\text{Fe}(\text{OH})_3}$; c) and Fe sulfides (J_{FeS_x} ; d) as implemented in the diagenetic model (site 4).

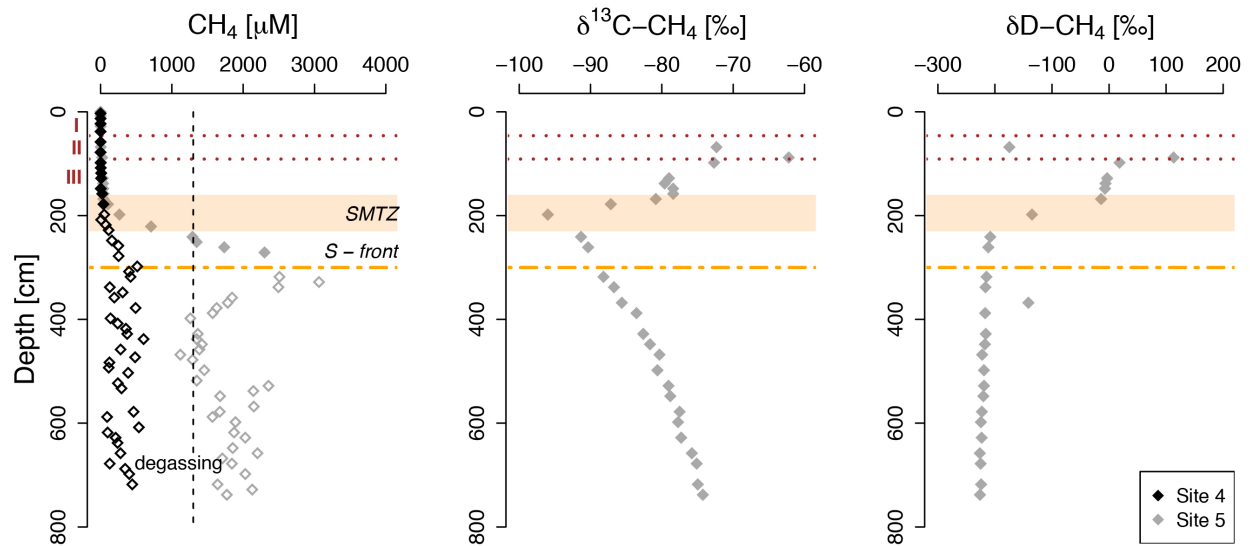
962



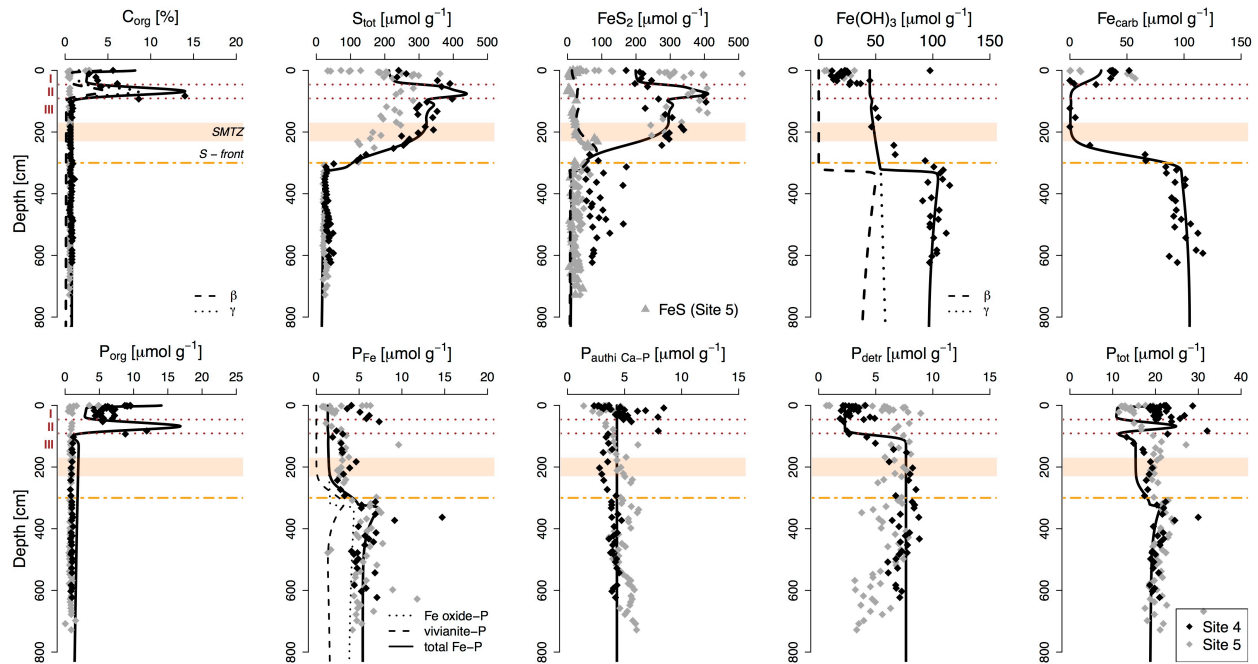
963
 964 **Figure 3. Pore water profiles of key components for site 4 (black diamonds) and site 5 (gray diamonds) and corresponding**
 965 **modeled profiles as calculated with the diagenetic model (black lines). Red dotted lines and roman numbers indicate the**
 966 **transitions between the lithological Unit I (modern coccolith ooze), Unit II (marine sapropel) and Unit III (limnic**
 967 **deposits). The orange bar represents the sulfate-methane transition zone (SMTZ) and the orange dashed line shows the**
 968 **current position of the downward migrating sulfidization front (S-front). The dashed vertical line indicates the CH₄**
 969 **saturation concentration at atmospheric pressure (Mogollón et al., 2013). The open diamonds indicate CH₄ concentrations**
 970 **that are likely underestimated due to outgassing of CH₄ during coring.**

971

972

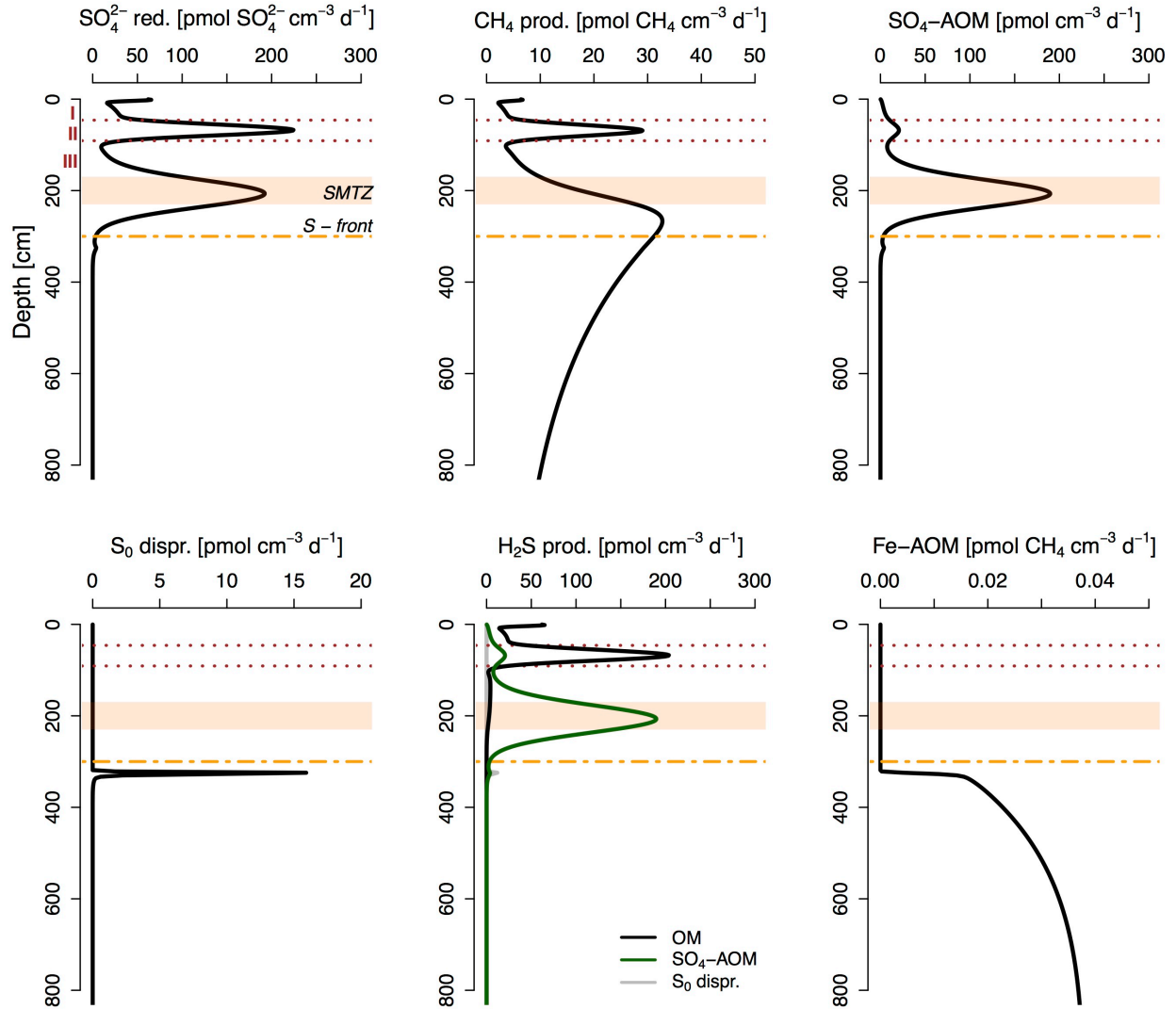


973
 974 **Figure 4. Pore water profiles of CH₄ for site 4 (black diamonds) and 5 (gray diamonds) and corresponding isotopic**
 975 **composition of dissolved CH₄ (available for site 5 only). δ¹³C-CH₄ values are given in ‰ vs. VPDB (Vienna Pee Dee**
 976 **Belemnite) and δD-CH₄ values are given in ‰ vs. V-SMOW (Vienna Standard Mean Ocean Water). Red dotted lines and**
 977 **roman numbers indicate the transitions between the lithological Unit I (modern coccolith ooze), Unit II (marine sapropel)**
 978 **and Unit III (limnic deposits). The orange bar represents the sulfate-methane transition zone (SMTZ) and the orange**
 979 **dashed line shows the current position of the downward migrating sulfidization front (S-front). The dashed vertical line**
 980 **indicates the CH₄ saturation concentration at atmospheric pressure (Mogollón et al., 2013). The open diamonds indicate**
 981 **CH₄ concentrations that are likely underestimated due to outgassing of CH₄ during coring.**
 982

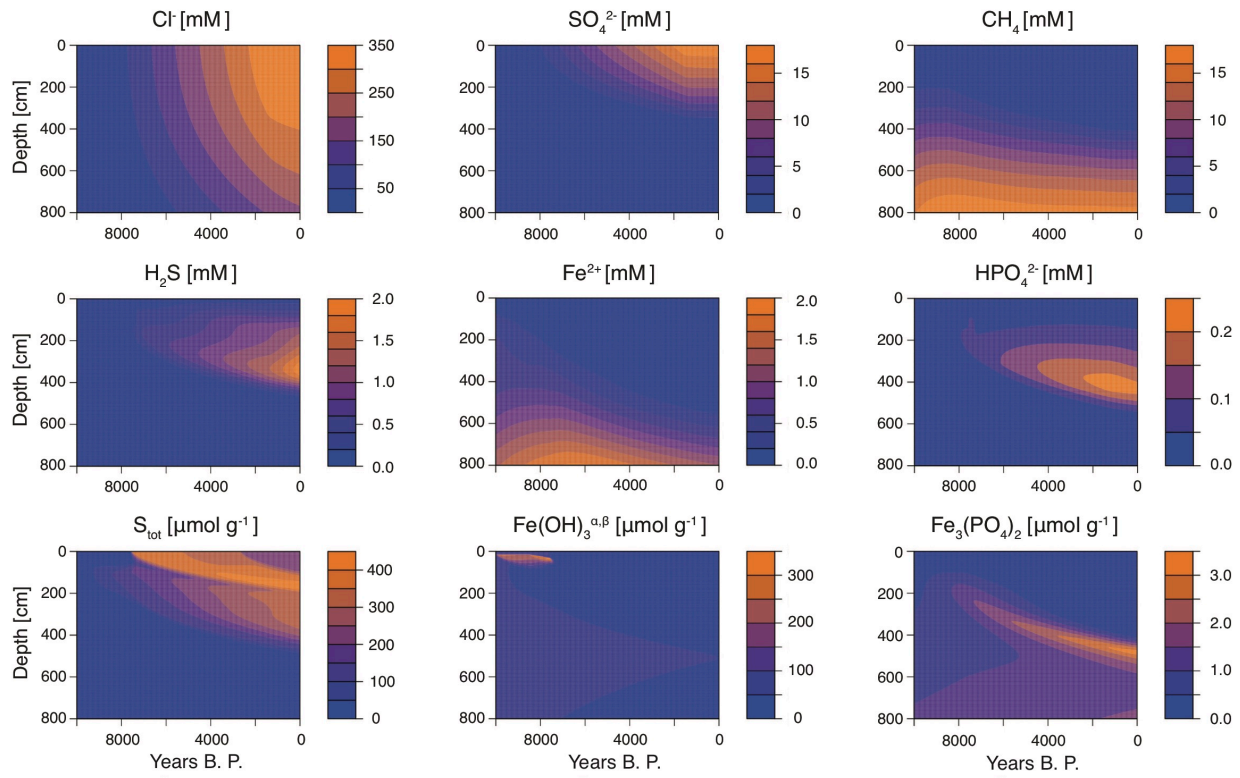


983
 984 **Figure 5. Solid phase sediment profiles for site 4 (black diamonds) and 5 (gray diamonds). Fe oxides represent the sum of**
 985 **amorphous, crystalline and recalcitrant oxides, i.e. Fe_{ox1} , Fe_{Ox2} and Fe_{mag} (Table 1, Supplementary Fig. S4). Fe_{carb} was**
 986 **corrected for apparent AVS dissolution during the Na acetate extraction step (the uncorrected Fe_{carb} data is given in**
 987 **Supplementary Fig. S4). Black lines represent profiles derived from the diagenetic model. Red dotted lines and roman**
 988 **numbers indicate the transitions between the lithological Unit I (modern coccolith ooze), Unit II (marine sapropel) and**
 989 **Unit III (limnic deposits). The orange bar represents the sulfate-methane transition zone (SMTZ) and the orange dashed**
 990 **line shows the current position of the downward migrating sulfidization front (S-front).**

991

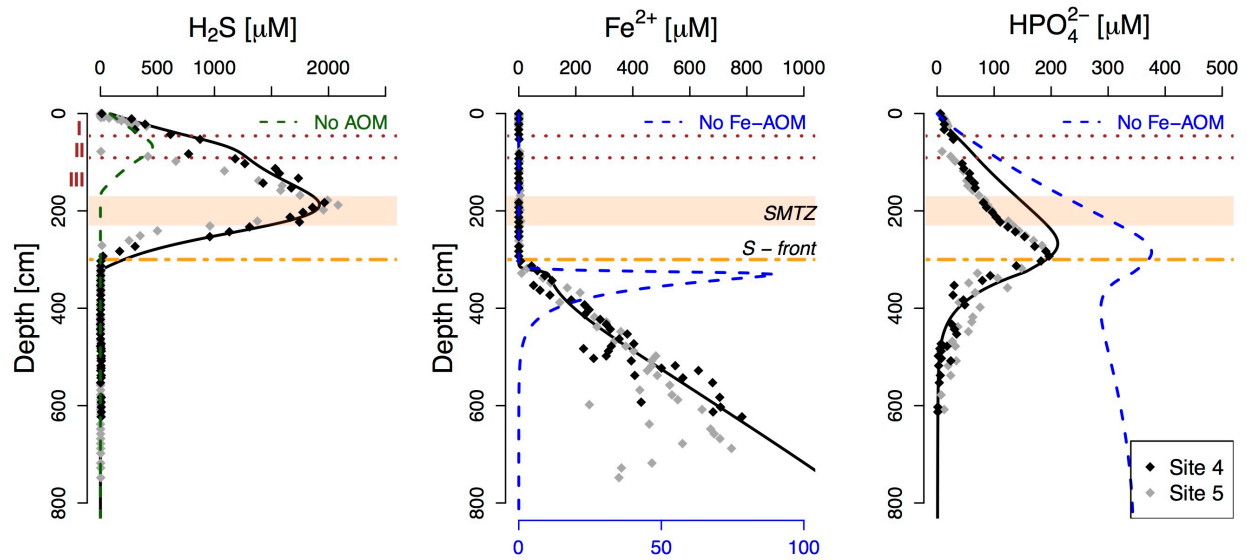


992
 993 **Figure 6. Modeled rates of total SO₄²⁻ reduction, total CH₄ production, SO₄-AOM, S₀ disproportionation, sulfide**
 994 **production and Fe-AOM. Red dotted lines and roman numbers indicate the transitions between the lithological Unit I**
 995 **(modern coccolith ooze), Unit II (marine sapropel) and Unit III (limnic deposits). The orange bar represents the sulfate-**
 996 **methane transition zone (SMTZ) and the orange dashed line shows the current position of the downward migrating**
 997 **sulfidization front (S-front).**
 998



999
 1000 **Figure 7. Transient evolution of selected pore water and sediment profiles with depth as calculated for site 4 using the**
 1001 **diagenetic model.**
 1002

1003



1004

1005

1006

1007

1008

1009

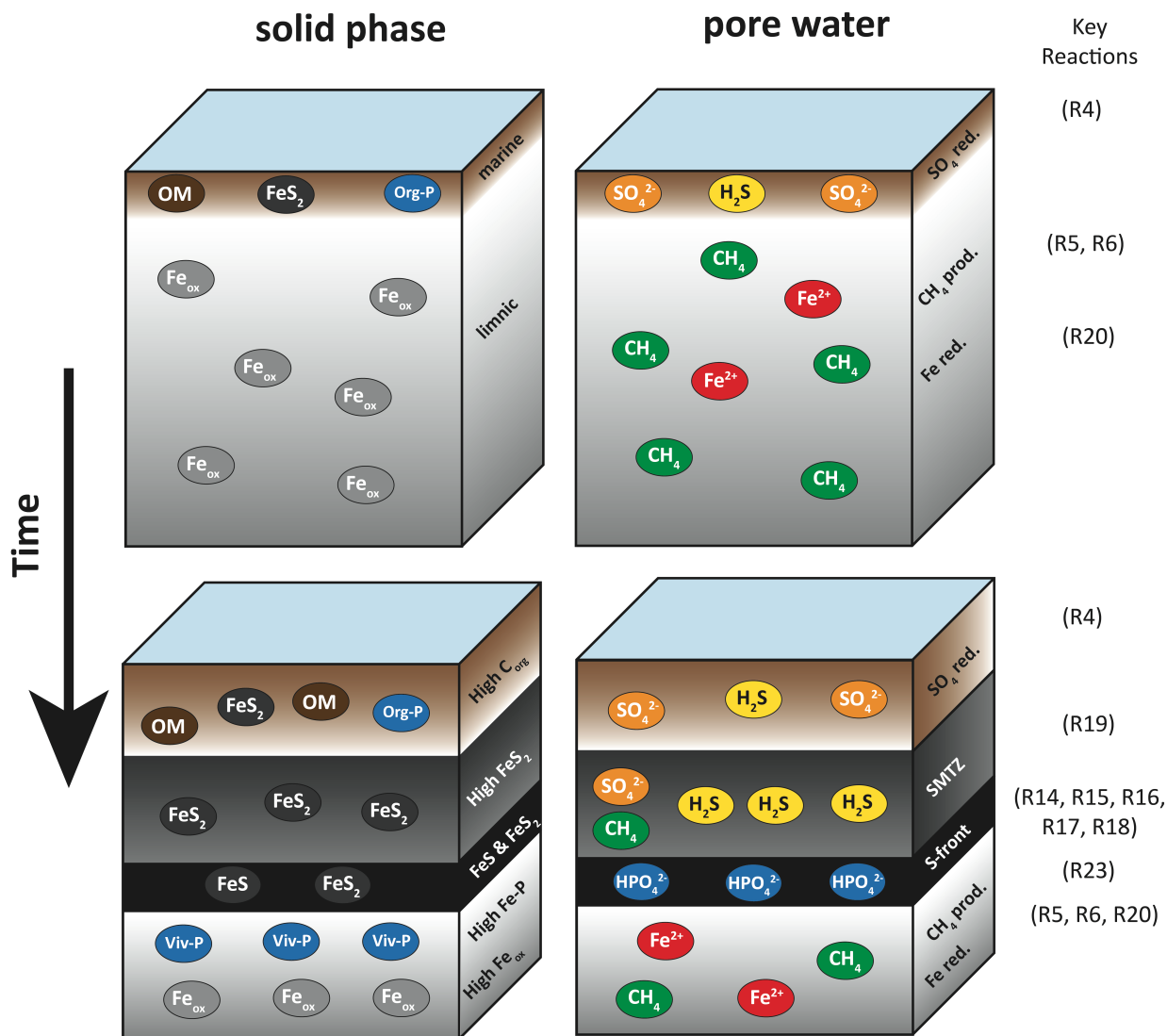
1010

1011

1012

1013

Figure 8. Pore water profiles of dissolved sulfide, Fe^{2+} and HPO_4^{2-} . The green dashed line represents the modeled sulfide profile without SO_4 -AOM, indicating that the latter significantly enhances the downward sulfidization. Blue dashed lines denote the modeled Fe^{2+} and HPO_4^{2-} profiles without ongoing Fe oxide reduction in the limnic deposits (i.e. no Fe-AOM). Note that concentrations of Fe^{2+} were multiplied 10 times in the model simulation without Fe oxide reduction to better visualize the potential release of Fe^{2+} through a cryptic S cycle (corresponding x axis at bottom). Red dotted lines and roman numbers indicate the transitions between the lithological Unit I (modern coccolith ooze), Unit II (marine sapropel) and Unit III (limnic deposits). The orange bar represents the sulfate-methane transition zone (SMTZ) and the orange dashed line shows the current position of the downward migrating sulfidization front (S-front).



1014
 1015 **Figure 9. Schematic of the main diagenetic processes discussed in this study and their imprint on the geochemical solid**
 1016 **phase (left) and pore water profiles (right). Accumulation of marine sediments with time and the subsequent downward**
 1017 **diffusion of SO₄²⁻ into the CH₄-bearing limnic sediment stimulate SO₄-AOM around the sulfate-methane transition zone**
 1018 **(SMTZ), thus enhancing the downward sulfidization of the Fe oxide-rich lake deposits. Below the sulfidization front (S-**
 1019 **front), HPO₄²⁻ released during reductive dissolution of Fe oxides is bound again in vivianite, leading to an enrichment in**
 1020 **sedimentary P in these sediments. Numbers on the right indicate the key reactions occurring in the corresponding**
 1021 **sediment layers as described in Table 3. Note that in this study, Fe-AOM (R20) was assumed as the main source of pore**
 1022 **water Fe²⁺ below the S-front to further test the potential impact of Fe-AOM on pore water CH₄. However, based on the**
 1023 **geochemical data, we cannot exclude a potential role for organoclastic Fe reduction (R3) and/or reactivation of less**
 1024 **reactive Fe oxides by methanogens.**